

Cy.5



## DEVELOPMENT OF HOLOGRAPHIC INTERFEROMETRIC APPLICATIONS IN THE VKF SUPERSONIC AND HYPERSONIC WIND TUNNELS

W. T. Strike, J. E. O'Hare, and W. L. Templeton  
ARO, Inc.

VON KÁRMÁN GAS DYNAMICS FACILITY  
ARNOLD ENGINEERING DEVELOPMENT CENTER  
AIR FORCE SYSTEMS COMMAND  
ARNOLD AIR FORCE STATION, TENNESSEE 37389

April 1975

Final Report for Period July 1, 1973 — October 20, 1974

Approved for public release; distribution unlimited.

Prepared for

DIRECTORATE OF TECHNOLOGY  
ARNOLD ENGINEERING DEVELOPMENT CENTER  
ARNOLD AIR FORCE STATION, TENNESSEE 37389

## NOTICES

When U. S. Government drawings specifications, or other data are used for any purpose other than a definitely related Government procurement operation, the Government thereby incurs no responsibility nor any obligation whatsoever, and the fact that the Government may have formulated, furnished, or in any way supplied the said drawings, specifications, or other data, is not to be regarded by implication or otherwise, or in any manner licensing the holder or any other person or corporation, or conveying any rights or permission to manufacture, use, or sell any patented invention that may in any way be related thereto.

Qualified users may obtain copies of this report from the Defense Documentation Center.

References to named commercial products in this report are not to be considered in any sense as an endorsement of the product by the United States Air Force or the Government.

This report has been reviewed by the Information Office (OI) and is releasable to the National Technical Information Service (NTIS). At NTIS, it will be available to the general public, including foreign nations.

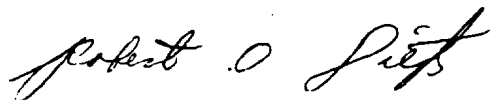
## APPROVAL STATEMENT

This technical report has been reviewed and is approved for publication.

FOR THE COMMANDER



MELVIN L. GUIOU  
Captain, USAF  
Research and Development  
Division  
Directorate of Technology



ROBERT O. DIETZ  
Director of Technology

# UNCLASSIFIED

REPORT DOCUMENTATION PAGE		READ INSTRUCTIONS BEFORE COMPLETING FORM
1. REPORT NUMBER <b>AEDC-TR-75-1</b>	2. GOVT ACCESSION NO.	3. RECIPIENT'S CATALOG NUMBER
4. TITLE (and Subtitle) <b>DEVELOPMENT OF HOLOGRAPHIC INTERFEROMETRIC APPLICATIONS IN THE VKF SUPERSONIC AND HYPERSONIC WIND TUNNELS</b>	5. TYPE OF REPORT & PERIOD COVERED <b>Final Report - July 1, 1973 - October 20, 1974</b>	
	6. PERFORMING ORG. REPORT NUMBER	
7. AUTHOR(s) <b>W. T. Strike, J. E. O'Hare, and W. L. Templeton, ARO, Inc.</b>	8. CONTRACT OR GRANT NUMBER(s)	
9. PERFORMING ORGANIZATION NAME AND ADDRESS <b>Arnold Engineering Development Center Arnold Air Force Station, Tennessee 37389</b>	10. PROGRAM ELEMENT, PROJECT, TASK AREA & WORK UNIT NUMBERS <b>Program Element 65802F</b>	
11. CONTROLLING OFFICE NAME AND ADDRESS <b>Arnold Engineering Development Center (DYFS) Arnold Air Force Station, Tennessee 37389</b>	12. REPORT DATE <b>April 1975</b>	
	13. NUMBER OF PAGES <b>41</b>	
14. MONITORING AGENCY NAME & ADDRESS (if different from Controlling Office)	15. SECURITY CLASS. (of this report)  <b>UNCLASSIFIED</b>	
	15a. DECLASSIFICATION/DOWNGRADING SCHEDULE <b>N/A</b>	
16. DISTRIBUTION STATEMENT (of this Report)  <b>Approved for public release; distribution unlimited.</b>		
17. DISTRIBUTION STATEMENT (of the abstract entered in Block 20, if different from Report)		
18. SUPPLEMENTARY NOTES  <b>Available in DDC</b>		
19. KEY WORDS (Continue on reverse side if necessary and identify by block number)  <b>holography interferometry wind tunnels</b>		
20. ABSTRACT (Continue on reverse side if necessary and identify by block number)  <b>This report summarizes the progress achieved in the von Kármán Gas Dynamics Facility (VKF) of the Arnold Engineering Development Center (AEDC), Air Force Systems Command (AFSC) to (1) improve the reconstruction process of holographic results, (2) develop diffuse, three-dimensional holography for use in the wind tunnel, and (3) prepare a data reduction program for converting interferometric results into meaningful static density</b>		

# UNCLASSIFIED

# UNCLASSIFIED

## 20. ABSTRACT (Continued)

distributions of a nonsymmetrical flow field. The report also contains some recommendations to make holography a more practical technique for recording optical results in the adverse environment existing around large supersonic and hypersonic wind tunnels.

## PREFACE

The work presented herein was performed at the Arnold Engineering Development Center (AEDC), Air Force Systems Command (AFSC) under Program Element 65802F. These results were obtained by ARO, Inc. (a subsidiary of Sverdrup & Parcel and Associates, Inc.), contract operator of AEDC, AFSC, Arnold Air Force Station, Tennessee. This research and development effort was conducted from July 1, 1973 to October 20, 1974, under ARO Project Numbers VF461 and V32Y-02A. The manuscript (ARO Control No. ARO-VKF-TR-74-103) was submitted for publication on October 23, 1974.

The programming and program analysis of the data reduction technique described in this report were performed by M. B. Krauth of the von Kármán Gas Dynamics Facility (VKF).

## CONTENTS

	<u>Page</u>
1.0 INTRODUCTION . . . . .	5
2.0 DEVELOPMENT OF LASER OPTICS AND RECORDING EQUIPMENT . . . . .	6
3.0 HOLOGRAPHIC TECHNIQUES . . . . .	9
4.0 INTERFEROMETRIC INVERSION TECHNIQUES . . . . .	21
5.0 CONCLUDING REMARKS . . . . .	36
6.0 RECOMMENDATIONS . . . . .	37
REFERENCES . . . . .	38

## ILLUSTRATIONS

### Figure

1.	Pulsed Ruby Laser System . . . . .	7
2.	Hologram Reconstruction System . . . . .	9
3.	Holographic Flow Visualization System . . . . .	10
4.	Holographic Finite Fringe Interferogram of Scarf Nozzle Plume . . . . .	10
5.	Diffuse Light Holographic System . . . . .	12
6.	Reflection Holographic Interferometry System . . . . .	13
7.	Diffuse Light Holographic Interferogram Reconstruction . . . . .	14
8.	Double Pulse-Diffuse Light Holographic Interferogram . .	15
9.	Infinite Fringe Interferogram (Diffuse Light) of a Sphere in a Mach 2.5 Stream ( $Re/ft = 9.3 \times 10^6$ ) . . . .	16
10.	Double Pulse-Diffuse Light Interferogram Fringes Representing Flow Changes against the Bottom Sur- face of the Model with a 400- $\mu$ sec Pulse Separation. . . .	17
11.	Finite Fringe Interferogram of a Sphere in a Mach 2.5 Stream ( $Re/ft = 9.3 \times 10^6$ ) . . . . .	19
12.	Double Pulse - Diffuse Light Holographic Inter- ferogram (700- $\mu$ sec Pulse Separation) . . . . .	20

<u>Figure</u>	<u>Page</u>
13. Initial Step of Interferogram Data Reduction . . . . .	22
14. Digitized Fringe Pattern of the Flow over a Sphere ( $M_\infty = 2.50$ and $Re/ft = 9.3 \times 10^6$ ) . . . . .	28
15. Minimum Shock Strength Required Assuming Flow Field Disturbance Produced an Optical Path Length to Fringe Shift Ratio of Ten . . . . .	30
16. Minimum Flow Deflection Angle Required Assuming Flow Field Disturbance Produced an Optical Path Length to Fringe Shift Ratio of Ten . . . . .	31
17. Analytically Defined Finite Fringe Pattern Produced by a 9-Deg Cone in a Hypersonic Stream at $\alpha = 0$ Using a Light Source with a Wave Length ( $\lambda$ ) of $0.6943 \mu$ . . . . .	32
NOMENCLATURE . . . . .	39

## 1.0 INTRODUCTION

During the past four or five years, progress has been made in the von Kármán Gas Dynamics Facility (VKF) in the development of a laser holographic system that will function adequately in the adverse environment surrounding a wind tunnel. The purpose of the present work was threefold, (1) to improve the procedure and equipment used to reconstruct holographic images, (2) to assess the feasibility of recording three-dimensional holographic results with a diffuse light source in the wind tunnel area, and (3) to provide a computer program for evaluating finite fringe holographic interferograms of nonsymmetrical flow fields.

As in the case of other studies of this nature, the problem of developing this optical method in a controlled environment such as an optics laboratory is usually easier than trying to adapt the same technique for use in and around a large wind tunnel. Wind tunnel vibration, thermal or density gradients produced by the heated tunnel circuit, long optical path lengths which are obviously dependent on the wind tunnel size, and dust or other air contamination all have an adverse effect on the holographic system. Although a pulsed laser of short duration minimizes the vibrational problem, it emits a relatively noisy beam with a short coherence length which produces a noisy electromagnetic wave front representation of the flow field image. In fact, the performance of the pulsed ruby laser now in use in the VKF optics laboratory varies at times in coherence and optical alignment between pulses. In an optics laboratory, a continuous wave (CW) laser with better coherence and an optically cleaner beam with a shorter optical path length can be used in a controlled, more stable environment to produce better holographic results. Some of the successful holographic techniques developed in the VKF optics laboratory which produced marginal results in the wind tunnel area will be described in this report along with some recommendations for obtaining improved optical results in the wind tunnel area.

In general, most holograms produced in VKF are obtained with a six-year-old pulsed ruby laser which is a relatively low-quality coherent light source with a wavelength of 0.6943 microns. The duration of the pulse is about 17 to 30 nanoseconds. This will freeze most fluctuations in an aerodynamic stream including most density fluctuations in a turbulent stream and eliminate any optical vibrational effects produced by the wind tunnel. The alignment of this laser and its coherence are not always well defined between pulses.



This document describes the accomplishments achieved in meeting the three major goals of this development program, namely (1) the improvements in the holographic reconstruction system, (2) the development of three-dimensional holography for use in the wind tunnel area, and (3) the programmed numerical inversion of holographically reconstructed interferograms.

## 2.0 DEVELOPMENT OF LASER OPTICS AND RECORDING EQUIPMENT

The holographic flow visualization techniques that have been developed at this facility since 1967 are documented in Refs. 1 through 5. In order to make these techniques operational in large wind tunnels which are used to obtain aerodynamic data, efforts were directed toward making the laser light source and optical system more reliable and improving the quality of the holographic recordings. Attention was also given to decreasing the time required to record and reconstruct holographic interferograms.

It is well known that the quality and reconstruction brightness of a hologram is directly related to the degree of coherence that a laser produces in its output beam. As a first step in improving the quality of the holograms, modifications and additions were made to a Q-switched ruby laser to improve the spatial and temporal coherence of the output beam, to make the operation more reliable, to improve the repeatability of the laser performance, and to reduce the irregularities in the output beam. The laser used on this project was a pulsed ruby laser with a Pockels cell Q-switch which was manufactured in 1968. The following steps were taken in an effort to bring this laser system shown in Fig. 1 up to an acceptable operational condition:

1. A new rear reflector was installed in the laser cavity. Repeated firing of the laser damages the mirror coating causing erratic lasing and a poor output beam intensity distribution.
2. The output reflector, a fixed sapphire etalon, was replaced with a three-surface coated sapphire etalon making it a temperature-tuned resonant component.
3. A transverse mode selector with a 2-mm-diam aperture mounted in a precision calibrated X-Y mount was added to the laser cavity.

4. An improved spatial filter-beam expander unit was installed in the laser output beam.
5. The water-to-air heat exchanger cooling system for the laser head was replaced with a refrigerated temperature-controlled system providing control to  $\pm 1$  °F.

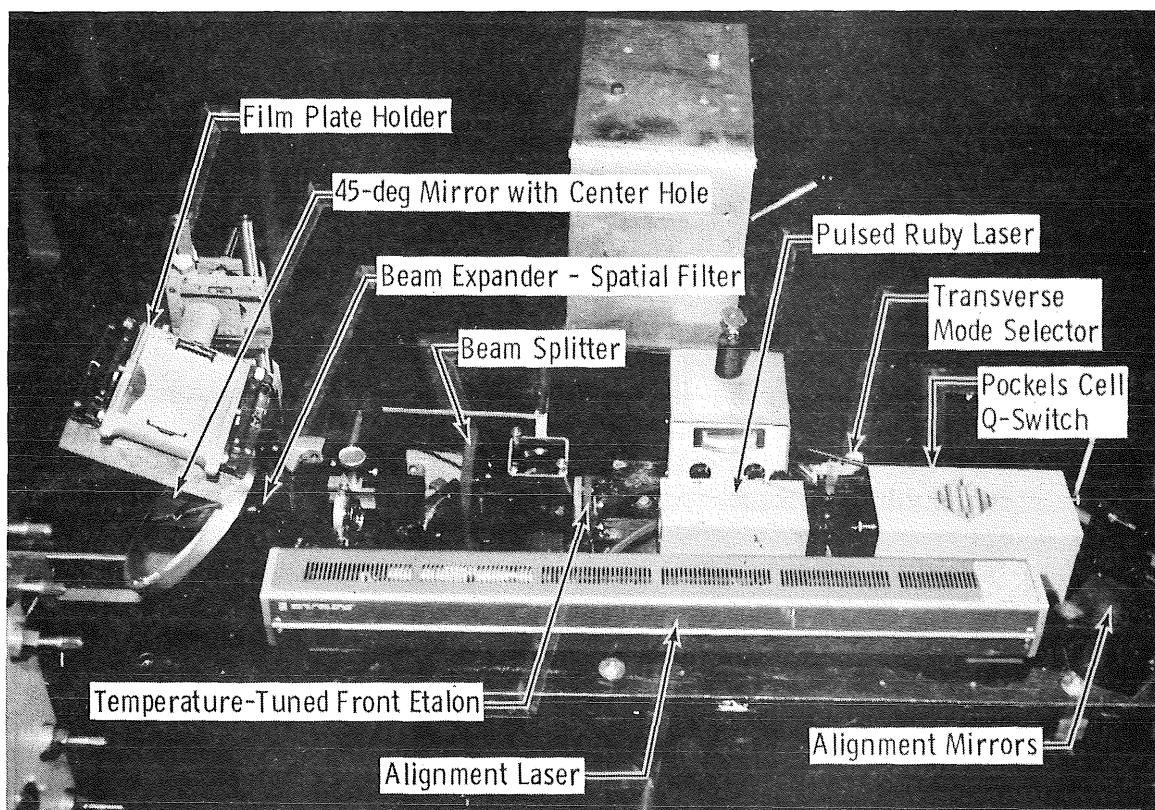


**Figure 1. Pulsed ruby laser system.**

The new rear reflector improved the uniformity of the laser beam considerably and the laser could be fired at lower energy levels permitting a greater range of control over the intensity of the laser beam. The tuneable, three-surface etalon permits selection of one of the several spectral lines which normally lase simultaneously through a Pockels cell Q-switched ruby laser. This greatly improved the temporal coherence of the laser beam, and its coherence length was determined experimentally to be approximately 30 cm. The refrigerated temperature-controlled cooling system for the laser head and the tuned etalon greatly improved the repeatability of the laser beam characteristics from shot to shot. The new spatial filter-beam expander unit

reduced the time required for alignment, and the spatial filter remained in alignment under the vibration conditions encountered around the wind tunnel.

The quality of the holograms recorded with this laser after the modifications were made was greatly improved, but the operation remained inconsistent and the repeatability left something to be desired. These problems are believed to be primarily due to the change in alignment of the optical components in the laser cavity caused by thermal contraction and expansion of the optical component mountings. This problem can possibly be solved by controlling the thermal environment of the aluminum mounts or replacing them with a material with a very low thermal coefficient of expansion.

Since reconstructing a hologram can be a time-consuming process, steps were taken to speed up this process and at the same time improve the quality of the reconstructed recordings. The following modifications were made to the reconstruction system shown in Fig. 2:

1. A 50-milliwatt (mw), CW, helium-neon (He-Ne) laser was installed in the reconstruction system to provide the coherent light source for the reference beam. The increased light output compared with the 15-mw He-Ne laser previously used decreased the exposure time required to record the reconstructed image. The operator is also able to focus the image accurately and make small interferometric fringe spacing adjustments with less eye strain.
2. A new double-hologram plate holder was fabricated and installed in the reconstruction system. This unit firmly holds two 4- by 5-in. glass plates and provides adjustments of one plate in relation to the other with six degrees of freedom. Precise alignment between the two plates is accomplished by the manual manipulation of the micrometer screw heads.
3. A diffraction limited collimator and spatial filter system was installed in the output beam of the He-Ne laser. This unit permits precise adjustment of the reference beam geometry so that the reference beam used for recording the hologram can be accurately duplicated.

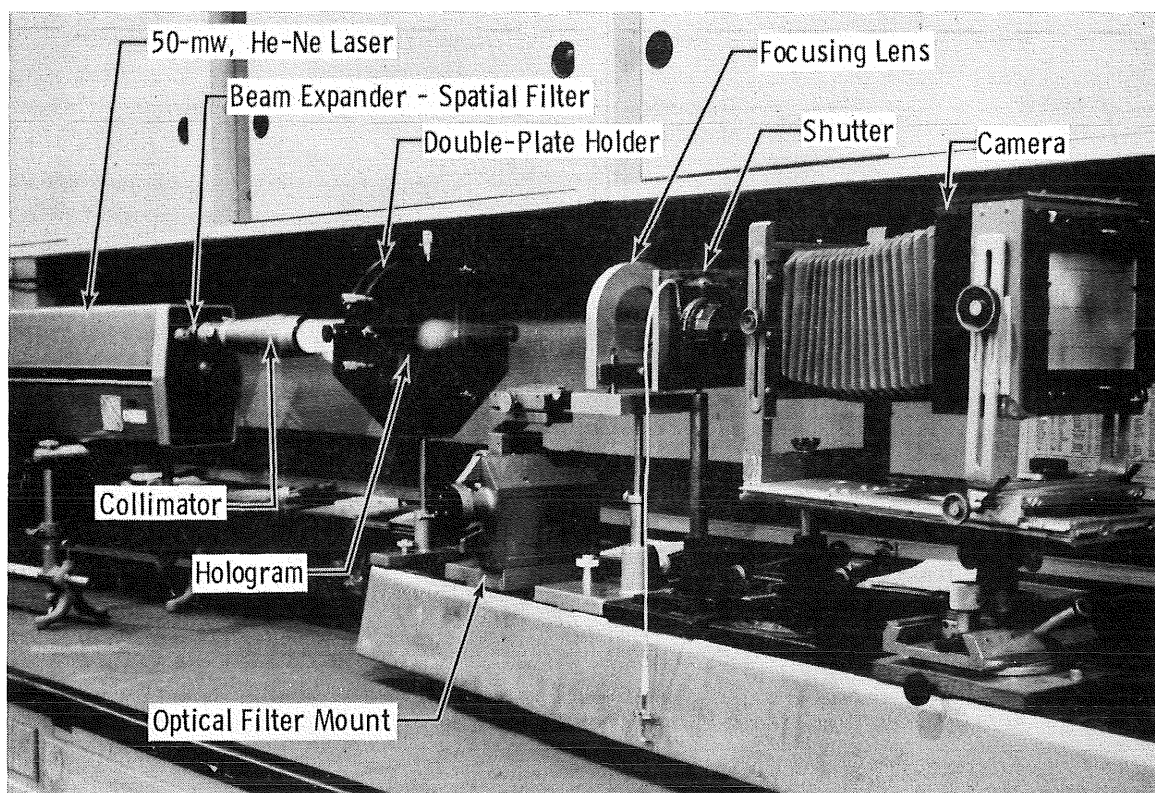


Figure 2. Hologram reconstruction system.

### 3.0 HOLOGRAPHIC TECHNIQUES

#### 3.1 DIRECTLY ILLUMINATED FLOW VISUALIZATION HOLOGRAPHY

This flow visualization technique using holography as the recording method has been documented in Refs. 1 and 3 and is shown schematically in Fig. 3. Using this method, a series of holograms were recorded of a nonsymmetrical jet plume exhausting into a wind tunnel test section in the absence of tunnel flow. The nonsymmetrical plume was produced by exhausting nitrogen gas through a scarf nozzle at a nozzle-to-tunnel chamber pressure ratio of 1400. The set of holograms shown in Fig. 4 consists of four views of the nonsymmetrical plume taken at 30-deg intervals. The nonsymmetry in the flow field is more apparent in the fringe pattern obtained at the 90-deg roll position (see Fig. 4). This was accomplished by rotating the scarf nozzle about its axis rather than changing the viewing angle of the optical system. The holograms were reconstructed using the finite fringe interferometric technique, and the fringe coordinates were read and digitized for the data reduction process outlined in Section 4.0. This technique is also applicable in obtaining multiple views of

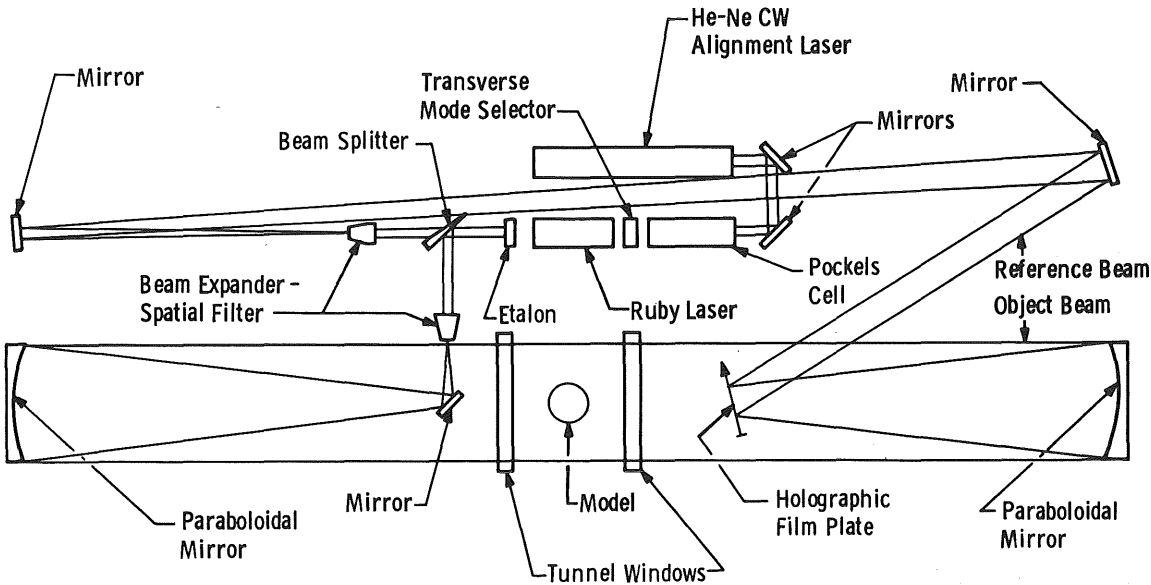


Figure 3. Holographic flow visualization system.



Figure 4. Holographic finite fringe interferogram of scarf nozzle plume.

axisymmetrical models in a flow field at angles of attack by rotating the model about the wind tunnel axis while maintaining the model angle with respect to the free-stream flow.

### 3.2 DIFFUSELY ILLUMINATED HOLOGRAPHIC INTERFEROMETRY

Theoretically, diffusely illuminated holographic interferometry offers a unique advantage over the directly illuminated interferogram in that the reconstructed fringes would be three-dimensional. This characteristic should eliminate the need to record several views of a nonsymmetrical flow field as outlined in Section 3.1. Since the fringes are three-dimensional, the angular views can be recorded during reconstruction of the hologram, limited only by the angle subtended by the film plate.

A diffuse light holographic system was constructed using a variation of the techniques that have been explored by others (Ref. 5). The holographic system is mounted on a heavy duty, portable, laboratory pedestal so that it can be easily moved from the laboratory to the wind tunnel. The portable unit shown in Fig. 5 includes all of the components required to produce reflected diffuse light holograms with the exception of the diffuser.

The Q-switched, pulsed ruby laser described in Section 2.0 is used to provide the coherent light source as shown in Fig. 1. A 15-mw He-Ne laser is auto collimated through the ruby laser on axis with the mode selector aperture to provide a continuous light source for alignment of the optical system. The continuous expanded light beam emitted from the optical system (shown in Fig. 6) also provides a means for aligning the portable holographic system with the area of interest in the wind tunnel test section.

A quartz, wedge beam splitter is located in the laser beam to provide two beams, one for the reference and one to illuminate the reflective diffuser (i. e., a beaded reflective surface) which is located behind the flow field in the wind tunnel test section. The reference beam, after being reflected 90 deg at the front surface of the beam splitter, is spatially filtered and expanded to fill a 4-in. -diam collimating lens. The collimated reference beam is then directed to the film plate at 20 deg from normal using three front surface mirrors. The front surface mirrors are mounted on optical benches so they can be adjusted to increase or decrease the reference beam optical path length to match the object beam path length. This feature provides the flexibility necessary for a portable holographic system



to be used in various sized wind tunnels. Typical optical path lengths that can be accommodated are from approximately two to fifteen feet.

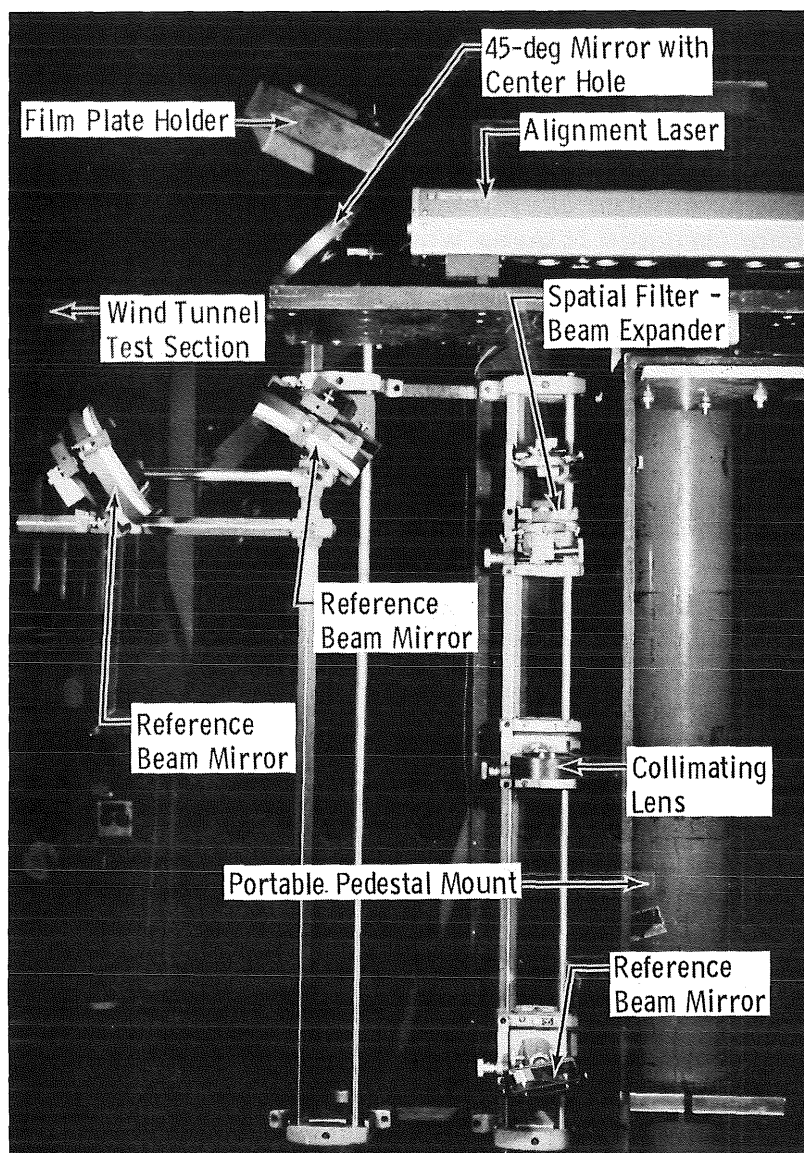


**Figure 5. Diffuse light holographic system.**

The portion of the laser beam that is transmitted through the beam splitter is also spatially filtered and expanded. After passing through a hole in the 45-deg front surfaced mirror, this beam (hereafter referred to as the object beam), provides the light to illuminate the reflection diffuser behind the flow field. The diffusely reflected light is collected by the 45-deg front surfaced mirror and reflected 90 deg to the film plate.

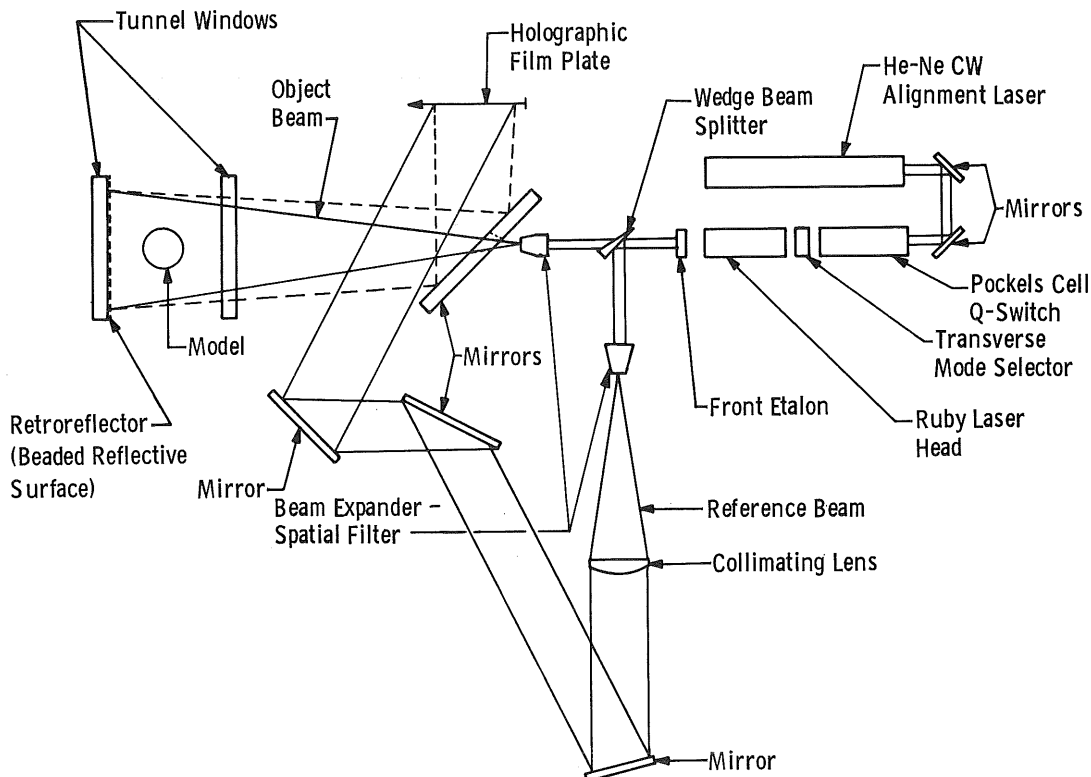


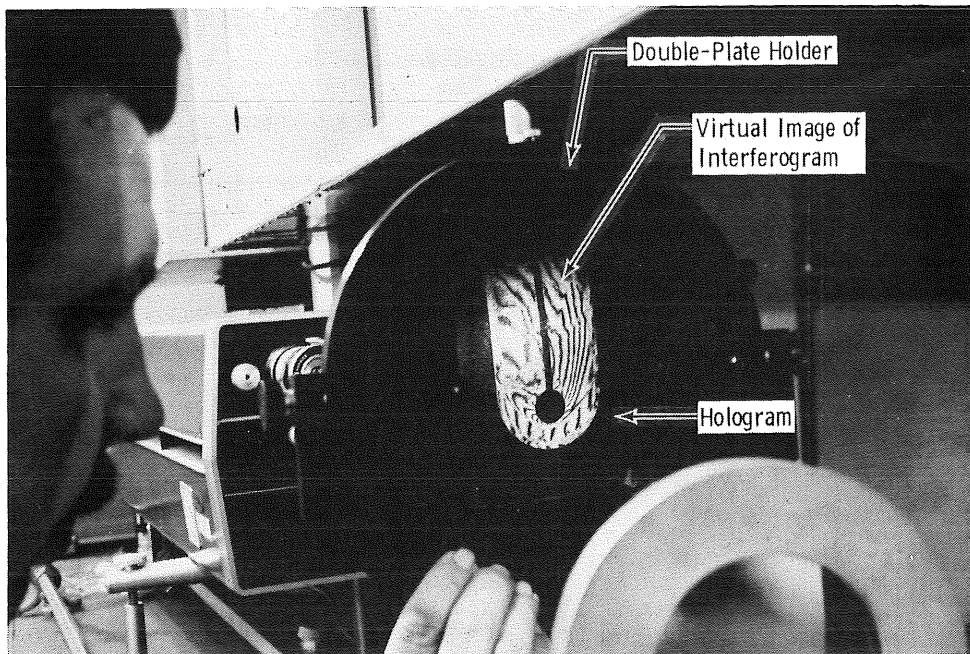
Figure 6. Reflection holographic interferometry system.

At this plane the object beam, with the flow field information, and the reference beam are combined to create the necessary interference to record the hologram.

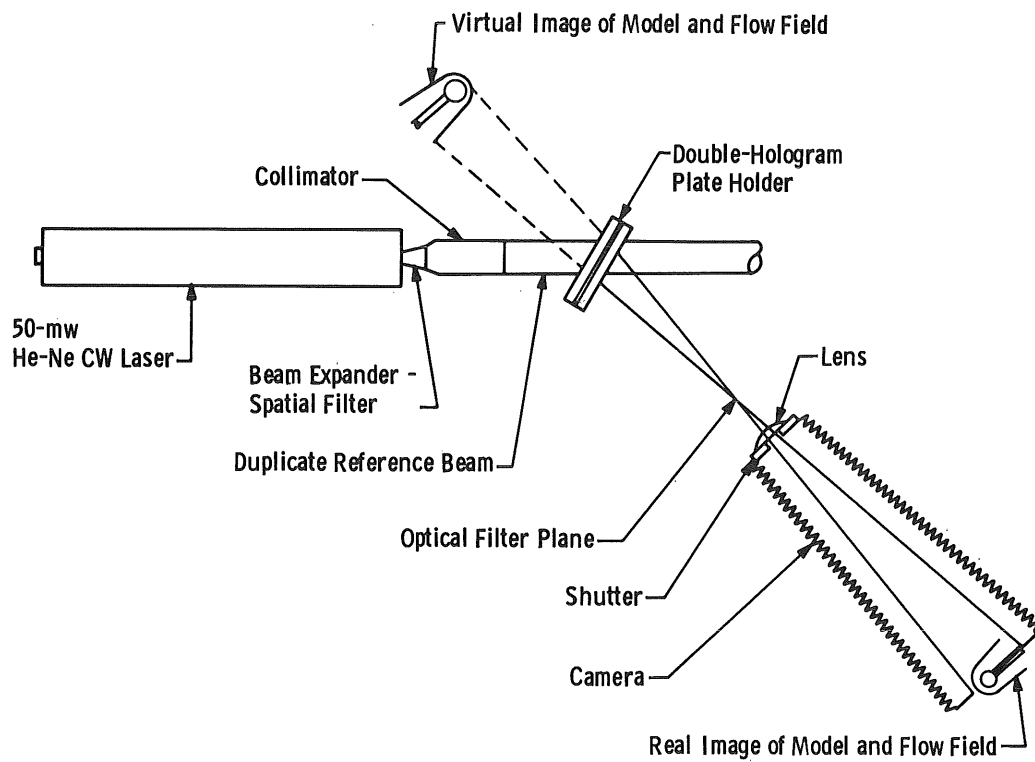
### 3.2.1 Experiments Using Diffuse Light Holographic Interferometry

When a diffuse light hologram is reconstructed, it produces an image of the area of interest against an illuminated background. The angle of view is limited by the size of the film plate used for the holographic recording and its distance from the area of interest. As shown in Fig. 7a the image is easily viewed with the unaided eye and is quite impressive; however, flow fields cannot be viewed using schlieren techniques as in the case of directly illuminated holograms. The components for this system are illustrated schematically in Fig. 7b. An interferometry technique must be employed to make the flow field visible and to provide the interferometric fringes necessary for quantitative evaluation.





a. Photograph of system



b. Components in the holographic reconstruction system

Figure 7. Diffuse light holographic interferogram reconstruction.

A double-exposed hologram shown in Fig. 8 provides an interferometric comparison of a flow field between the two separate instances in time at which the two exposures were made. In most cases, it is desirable to compare a flow field disturbance (such as the flow about a wind tunnel model) with the undisturbed flow field (with no model present.)

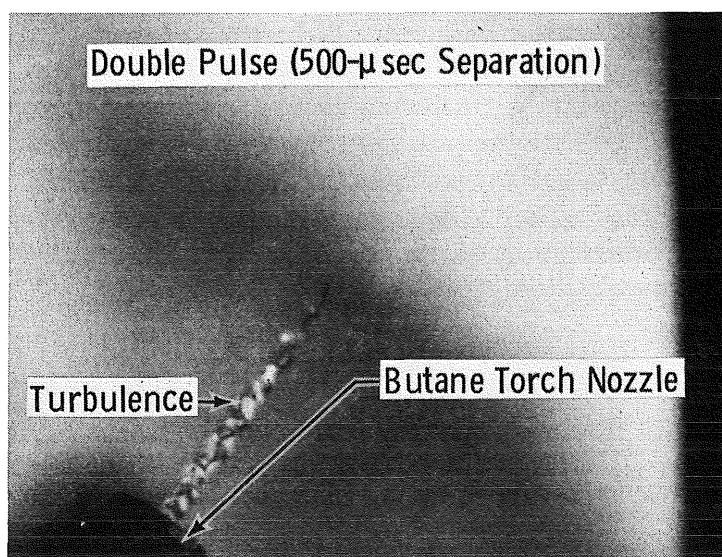
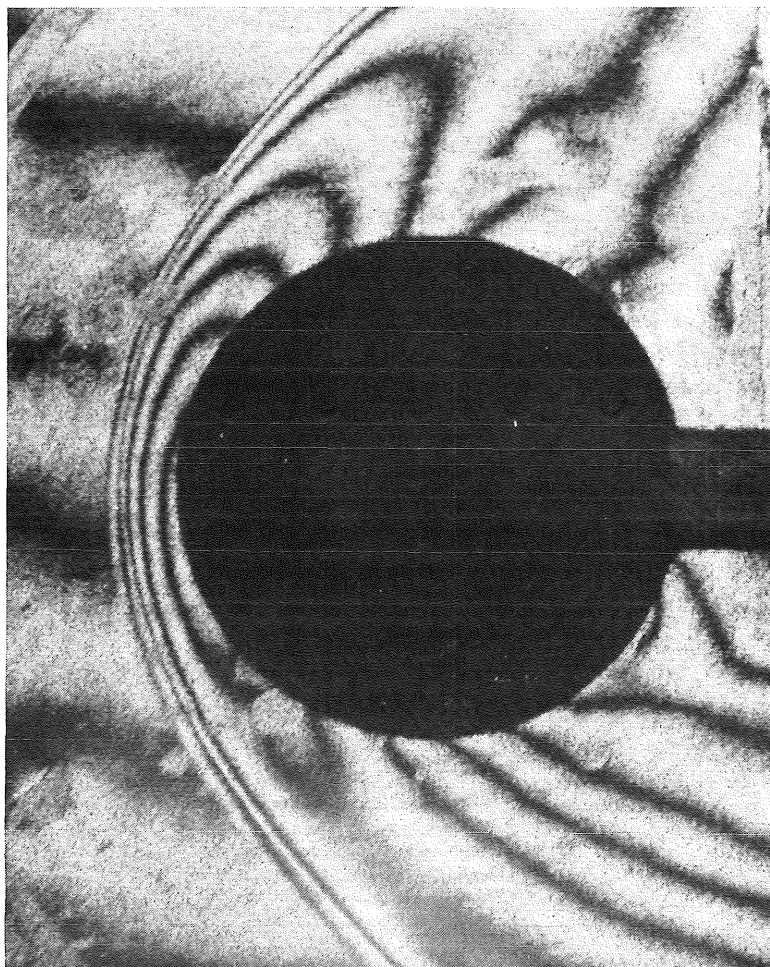


Figure 8. Double pulse-diffuse light holographic interferogram.

Several double-exposure methods are possible, all of which produce essentially the same results. However, in a non-laboratory environment, most of these techniques can be immediately eliminated. Unlike the directly illuminated holographic interferogram, fringes are not detectable if movement occurs between the holographic image and the diffuser by as much as one wavelength between the two exposures. This restraint also suggests that it is not possible to precisely align two separate diffuse light holograms during the reconstruction process as can be accomplished with directly illuminated holograms (Ref. 3). An effort was made to develop a technique to accomplish the precision alignment necessary to produce fringes. Although this effort was not successful, it is not believed to be an impossible task; considering the benefits that could be derived from such a technique, it deserves further investigation.

Experiments were conducted using the double-exposure technique on a single film plate. In order to compare a flow field in its disturbed versus undisturbed condition, sufficient time is required to remove the disturbance from the flow field between exposures. This is possible under laboratory conditions and in a small wind tunnel where vibration

is not a problem. An example of this type of holographic interferogram is shown in Fig. 9. The first exposure was made with the model removed from the wind tunnel test section (Tunnel D, which has a 12- by 12-in. test section) and a beaded reflective surface covering the opposite window. A hemisphere model was then installed, the tunnel brought to operating conditions, and the second exposure made. Approximately five minutes elapsed between the two exposures. The resulting fringes are a comparison between the undisturbed and disturbed flow field. Although care was taken not to move the diffuser between exposures, it is obvious in Fig. 9 that small areas of the diffuser moved causing fringe discontinuity and making that portion of the data unusable. This experiment was made under ideal conditions which are not normally found around a larger operational wind tunnel; therefore, this technique is not considered to be useful except under ideal conditions.



**Figure 9. Infinite fringe interferogram (diffuse light) of a sphere in a Mach 2.5 stream ( $Re/ft = 9.3 \times 10^6$ ).**

A solution to the problem of movement between exposures is to make the two exposures at essentially the same instant. This technique was used with some success in the environment around a larger wind tunnel (such as the VKF Tunnel A which has a 40- by 40-in. test section with exposure separations up to one millisecond. The results are shown in Fig. 10. Since it is physically impossible to inject or remove a model from the flow field during such a short time span, one must settle for comparing the flow field differences existing between the time intervals selected with the model in a fixed position. In most cases, flow field variations occurring in one millisecond or less might be attributed to

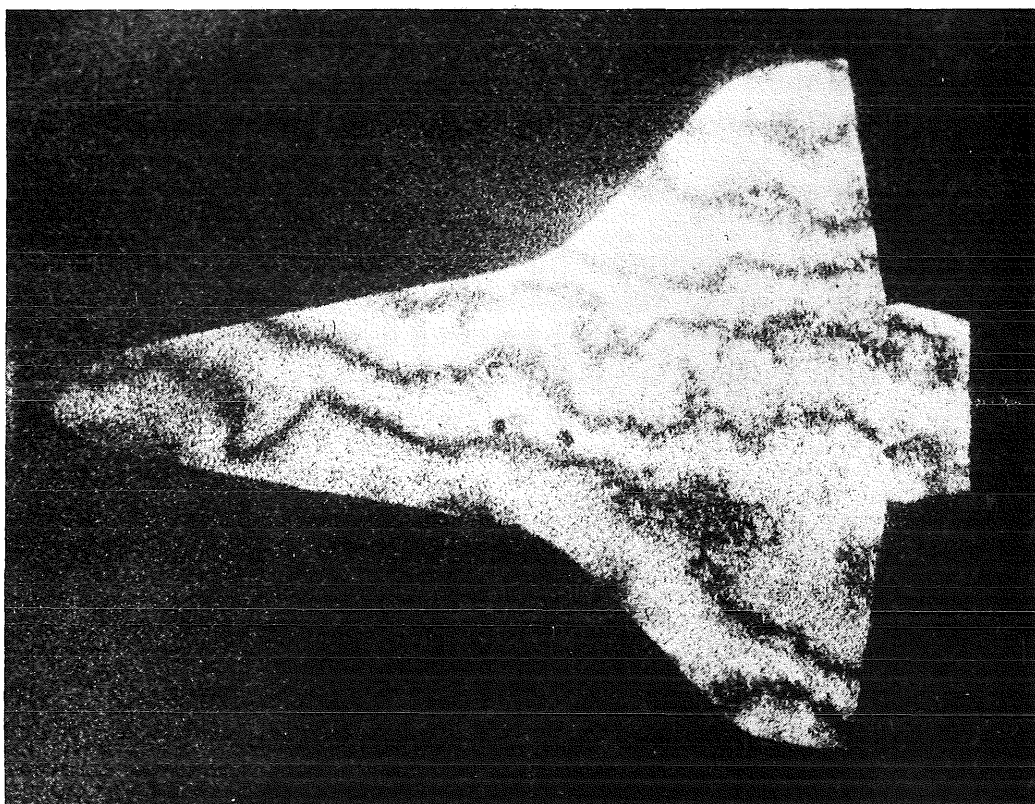


**Figure 10. Double pulse-diffuse light interferogram fringes representing flow changes against the bottom surface of the model with a 400- $\mu$ sec pulse separation.**

flow field turbulence. A steady-state flow field will not produce interference fringes using this technique since the density distribution in the flow field remains essentially the same between the two exposures. In Fig. 10, these fringe patterns reflect the flow field turbulence existing over the model surface superimposed on the optical noise attributed to the vibration of the model, the optical system, and possibly the tunnel structure.

An interesting possibility provided by the reflected diffuse light technique is the ability to record the flow field in corners which are normally in a shadow region when using conventional flow visualization methods. An example would be the visualization of the flow field at the intersection of a wing root and the fuselage of an aircraft. In this case the diffuser would be placed on the fuselage or the wing surface of the aircraft model.

Another ideal application for this technique is in the flow field visualization of models in high-velocity, free-flight tests. The first exposure could be made of the undisturbed flight path just before the model arrives in the field of view and the second exposure made within microseconds as the model and the resulting flow field disturbances arrive in the field of view.

### **3.2.2 Hologram Reconstruction Experiments**

The basic requirements for the reconstruction of diffuse light holograms are essentially the same as for the directly illuminated holograms (Ref. 1). A coherent light source must be used, and the geometry of the beam (or the light waveform) must be a reproduction of the reference beam used to record the hologram as shown previously by the system in Fig. 7b.

There is one major difference in the reconstruction of directly illuminated and diffusely illuminated holograms where interferometric fringes are to be formed and recorded. With a directly illuminated hologram, the reconstructed fringes exist throughout the object beam and are in focus in the flow field disturbance plane. This is not the case with diffusely illuminated holograms. The fringes are not usually located in the plane of the flow field disturbance and are located at infinity in many cases. The fringes appear to be located in the proper plane when viewing the reconstructed virtual image with the eye due to its small aperture; therefore, when photographing the reconstructed image, it is necessary to use a small aperture in the camera lens to obtain the required depth of field to record both the model and the fringes in sharp focus.

### **3.2.3 Comparison Between Directly Illuminated and Diffusely Illuminated Holographic Interferograms**

A series of holograms were recorded in the VKF Supersonic Tunnel D to compare directly illuminated and diffusely illuminated holographic techniques. A 2.247-in. -diam hemisphere model was used in

this blowdown tunnel at Mach 2.5. Figure 9 is a diffuse light infinite fringe interferogram recorded using the technique described in Section 3.2.2. Figure 11 is a directly illuminated finite fringe interferogram

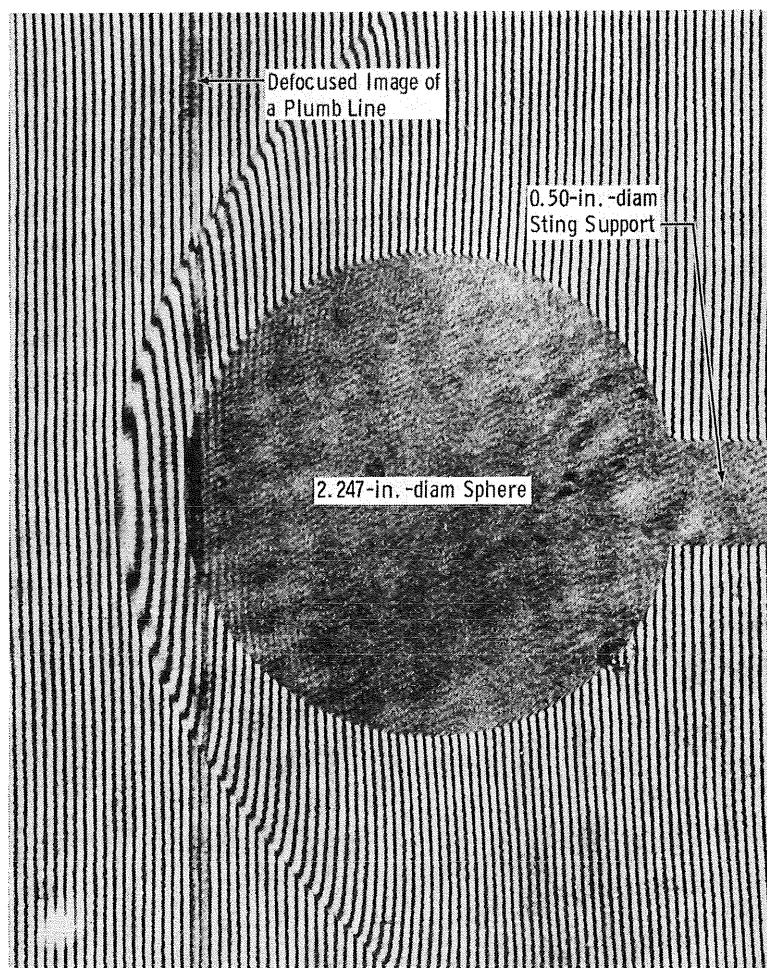


**Figure 11. Finite fringe interferogram of a sphere in a Mach 2.5 stream ( $Re/ft = 9.3 \times 10^6$ ).**

recorded using the double-exposure technique described in Ref. 2. Figure 12 is a double pulse (700- $\mu$ sec separation)-diffuse light infinite fringe interferogram recorded using the technique previously described. The three types of holographic interferometric recordings were made at the same tunnel conditions (Mach 2.5 and  $Re/ft = 9.3 \times 10^6$ ). The fringes in Fig. 12 supposedly indicate a high-frequency turbulence in the tunnel free stream that obliterated fringes that should occur in the turbulent area in the wake of the hemisphere. It is interesting to note that fringes formed on Scotchlite<sup>®</sup> that was placed on the model sting, and this indicates that the sting was vibrating as the hologram was recorded.



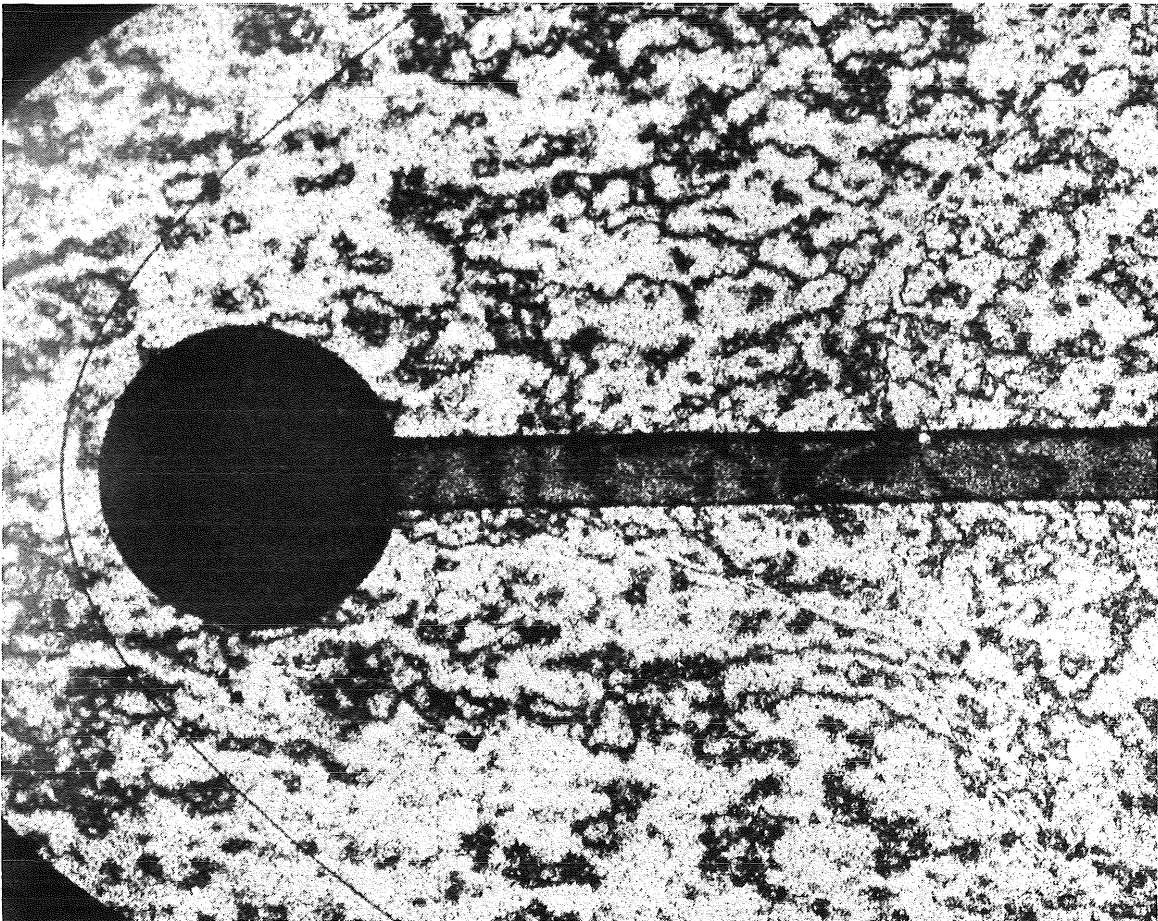


**Figure 12. Double pulse—diffuse light holographic interferogram  
(700- $\mu$ sec pulse separation).**

A summary of the advantages and disadvantages of diffuse light holographic interferometry are listed below:

Advantages:

1. The reconstructed interferometric fringes are three dimensional and the angle at which they can be viewed is limited only by the size of the hologram.
2. Interferometric fringes can be produced of flow fields in corners or against opaque backgrounds which is impossible using conventional flow visualization methods.
3. Fringes created by flow fields are easily viewed against an illuminated background with the unaided eye.

Disadvantages:

1. Interferometric fringes are diffused, have low contrast, and are not well defined.
2. Fringes are difficult to record during reconstruction due to their localization in respect to the model image.
3. The optical system and the diffuser (i. e., the surface covered in this case with a beaded reflective surface) must not move more than one wavelength between exposures.
4. At the present time, it is difficult to differentiate between fringes caused by optical system movement and those caused by density changes in the flow field.

After evaluating the results of many tests in the laboratory and under actual operating conditions in large supersonic and hypersonic wind tunnels (such as the VKF Tunnels A, B, or C), it is believed that directly illuminated holographic interferometry is the most useful technique with the technology presently available. Diffuse light holographic interferometry may be useful in specialized cases. Its usefulness would be greatly increased with the development of techniques to record the reference and test holograms on separate plates and reconstruct them simultaneously in a laboratory environment.

#### 4.0 INTERFEROMETRIC INVERSION TECHNIQUES

The differential holographic technique utilizing a pulsed ruby laser provides a useful method producing infinite and finite fringe interferograms of flow fields recorded in the adverse environment surrounding a wind tunnel facility. The physical principles involved in the generation of optical fringe patterns are adequately documented in many technical volumes such as Refs. 6 and 7. In the present application, using the directly illuminated light source technique, two holograms which are the photographic film records of the electromagnetic signal (i.e., its amplitude and phase angle) of an optical wavefront of an image illuminated by a coherent light source are used to produce a fringe pattern. One hologram contains a record of the flow field disturbance while the second contains a record of the flow field with the disturbance removed. In the wind tunnel, this means one hologram is obtained with the model in the wind tunnel flow and a second with the model or disturbance removed.



In some cases, both these records or exposures are recorded on a single holographic plate which when reconstructed produces the optical interference fringe patterns corresponding to the change in the flow field static density distribution. If the holographic plate remains in an optically fixed position between the exposures, the reconstruction will produce an infinite fringe pattern, whereas a shift in the holographic plate between the two exposures will produce a finite fringe pattern when the image is reconstructed.

#### 4.1 NUMERICAL SCHEME FOR AXISYMMETRIC FLOW FIELDS

The shift in the fringe pattern  $F(\theta, Z)$ , that is, the magnitude of the nonuniformities in a fringe pattern similar to the one shown in Fig. 13 can be accurately (mathematically speaking) related to the variation in

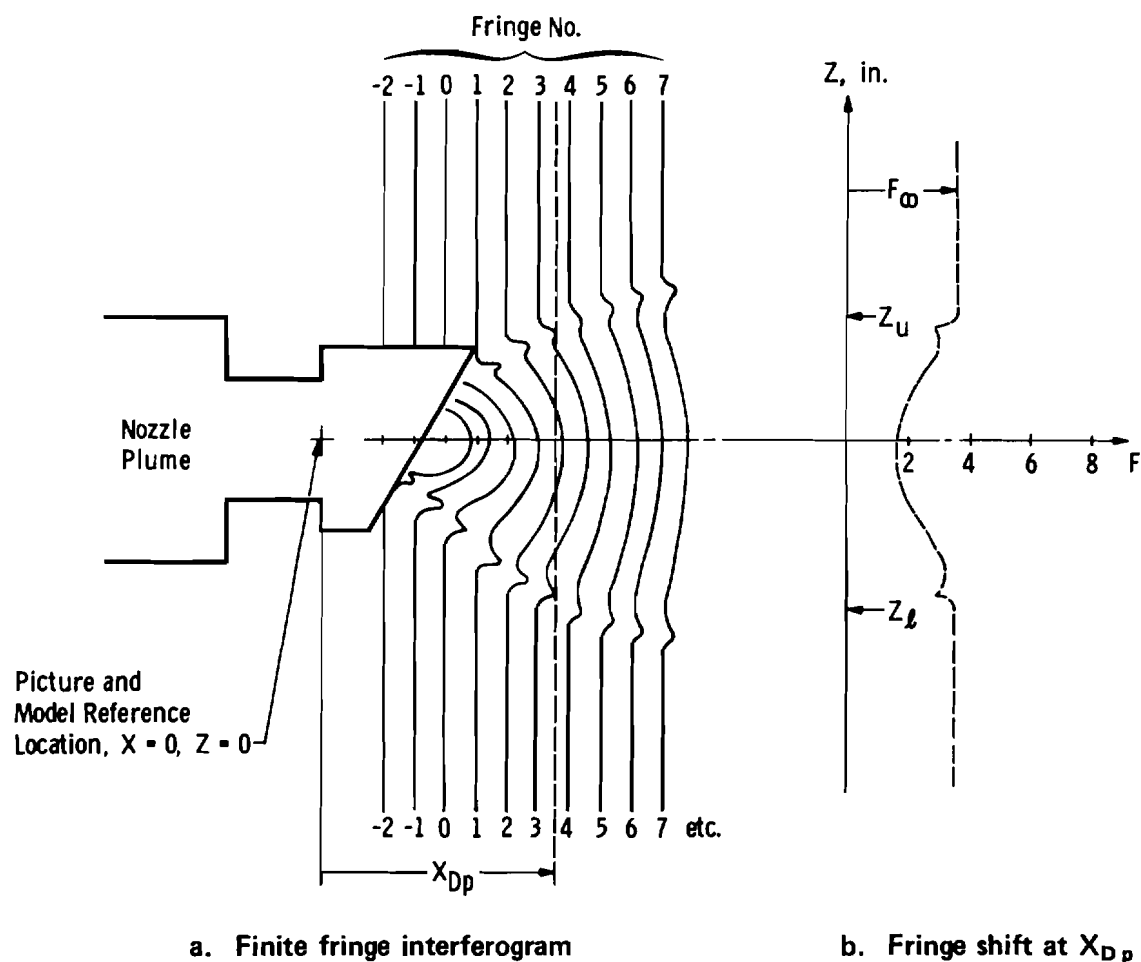


Figure 13. Initial step of interferogram data reduction.

the static density,  $\rho(Y', Z')$ , along an optical path length,  $Z$ , by the following expression:

$$F(\theta, Z) = (K/\lambda) \int_{Z_\ell}^{Z_u} [\rho(Y', Z') - \rho_\infty] dZ \quad (1)$$

where  $\rho(Y', Z') - \rho_\infty = 0$  when  $Z > Z_u$  or  $Z < Z_\ell$ . The constant  $K$  is the Gladstone-Dale constant and  $\lambda$  is the wave length of the light source. Since the fringe number distribution  $F(\theta, Z)$  can be defined from the interferogram, a numerical procedure must be selected to invert this expression so that the density distribution can be evaluated in terms of the fringe shift distribution.

As suggested in Fig. 13a, the initial step consists of systematically assigning consecutive numbers to the fringe lines. Then a data plane must be selected at a point where the flow field density distribution is desired. An interpolation scheme is then employed to define the fringe number distribution along this data plane as suggested in Fig. 13b. The fringe shift distribution  $F(\theta, Z)$  is then defined as the difference between a reference fringe value, in this case  $F_\infty$ , and the fringe value within the region of the flow field disturbance.

If the flow field is known or assumed to axisymmetric, the above expression (Eq. (1)) can be written in the form of Abel's equation. The density distribution is assumed to be independent of the angular coordinate  $\theta$  and only dependent on the radial coordinate,  $Z$ . At any given data plane location, the maximum radius of the disturbance is denoted as  $R$ . Therefore, Eq. (1) reduces to the following form:

$$F(Z) = (K/\lambda) \int_Z^R [\rho(r) - \rho_\infty] / \sqrt{r^2 - R^2} d(r^2) \quad (2)$$

and  $\rho(r) = \rho_\infty$  when  $r > R$  and  $F(Z) = 0$ .

The following substitutions were made by Bradley (Ref. 8) into this equation:

$$T = 1 - (Z/R)^2 \quad (3a)$$

$$V = 1 - (r/R)^2 \quad (3b)$$

and

$$A = K/(\lambda R) \quad (3c)$$

The fringe shift distribution was curve fitted with the following polynomial:

$$F(T) = \sqrt{T} \sum_{n=0}^3 B_n T^n \quad (4)$$

Abel's equation can now be solved by means of Laplace transforms and this mathematical scheme provides the inversion technique to define the density distribution of an axisymmetric flow field disturbance in terms of a known fringe shift distribution. As formulated in Ref. 8, the numerical procedure defining the inversion of Abel's equation has the following form:

$$\rho(T) - \rho_{\infty} = (1/A) \sum_{n=0}^3 B_n [1 \cdot 3 \cdot 5 \cdots (2n+1) T^n / (2^{n+1} n!)] \quad (5)$$

Near the outer limit of the disturbance (i.e., as  $T \rightarrow 0$  or  $Z \rightarrow R$ ), this solution produces a density difference, namely  $\rho(T) - \rho_{\infty}$ , which corresponds to a density increment or bow wave strength existing at the boundary of the flow field disturbance,

$$\rho(T \rightarrow 0) - \rho_{\infty} = B_0/(2A) \quad (6)$$

This procedure for inverting Abel's equation was adopted and modified slightly by requiring the polynomial curve fit (Eq. (4)) to apply to five adjacent points in the fringe shift distribution rather than attempting to fit the entire distribution. These five points were used to define the incremental change in density occurring between the first two points in the group of five points. This procedure begins at the outer edge of the disturbance and finishes at the center and acts as a smoothing procedure for the data and improves the evaluation of the static density distribution.

## 4.2 NUMERICAL SCHEME FOR ASYMMETRIC FLOW FIELDS

A more general method of inverting Eq. (1) for nonsymmetrical and symmetrical flow fields was formulated by Collins and Jagota (Ref. 9) using an analytical approach of Maldonado and Oslen (Ref. 10). The method uses orthogonal polynomials which remain "invariant in form" during the rotation of a coordinate system. The development of these interrelated polynomials is described in Ref. 11 by Maldonado. The formal mathematical development of this numerical inversion technique will not be presented, but the fundamental expressions used in the numerical analysis will be summarized.

The integral expression is initially simplified to the following form:

$$G(Z, \theta) = \int_{Z_1}^{Z_u} f(Y', Z') dZ \quad (7)$$

where

$$G(Z, \theta) = F(Z, \theta) \lambda / (K \rho_{\infty})$$

and

$$f(Y', Z') = (\rho(Y', Z') / \rho_{\infty}) - 1$$

The angle  $\theta$  represents the coordinate of rotation of the wind tunnel (or flow field) coordinates ( $Y'$  and  $Z'$ ) with respect to the coordinates of the plane in which the fringe patterns were recorded. The integral expression is now nearly identical to the equation used by Maldonado and Olsen to deduce the emission coefficient from the measured emitted spectral intensity distribution of a nonsymmetrical plasma source.

Two polynomials which are invariant in form to a rotation of coordinates, orthogonal to the Gaussian weighting function  $e^{-(\alpha r)^2}$  (where  $r^2 = (Y')^2 + (Z')^2$ ) and related by means of the following integral are used in this analysis

$$\int_{-\infty}^{\infty} U_{2p+n}^{+n}(\alpha Y', \alpha Z') e^{-(\alpha Y')^2} dY = \frac{e^{\pm i n \theta} H_{2p+n}(\alpha Z)}{\sqrt{p! (n+p)!} 2^{(2p+n)}} \quad (8)$$

where

$$U_{2p}^{+n}[(\alpha r)^2] = (-1)^p \frac{\alpha}{\sqrt{\pi}} \left[ \frac{p!}{(n+2p)!} \right]^{1/2} (\alpha r)^m e^{\pm i n \theta} L_p^n(\alpha r)^2$$

and

$$\phi = \tan^{-1}(z/y) \text{ and } r^2 = Y^2 + Z^2$$

The expression  $L_p^n[(\alpha r)^2]$  is a Laguerre polynomial while  $H_{2p+n}(\alpha Z)$  is a Hermitain polynomial. Only the real components of these complex polynomials are used in this analysis.

$$f(Z', \theta) = \left(\frac{\alpha}{\pi}\right)^2 \sum_{n=0}^N \sum_{p=0}^P \frac{\epsilon_n (-1)^p p!}{(n+2p)!} (ar)^n e^{-(ar)^2} L_p^n (ar)^2 \left[ B_{n+2p}^n(\alpha) \cos n\phi + D_{n+2p}^n(\alpha) \sin n\phi \right] \quad (9)$$

where

$$L_p^n [(ar)^2] = \sum_{s=0}^p (-1)^s \frac{(p+n)!}{(p-s)! (n+s)! s!} [(ar)^2]^s \quad \text{and}$$

$$\epsilon_n = \frac{1}{2} \text{ if } n = 0 \text{ and } \epsilon_n = 1 \text{ for } n > 0$$

The function  $f(Z', \theta)$  represents the differential static density ratio, namely  $(\rho(Z', \theta)/\rho_\infty - 1)$  which is the final result produced by this numerical inversion technique. When the requirement for orthogonality was applied to this polynomial, then the coefficients  $B_{n+2p}^n(\alpha)$  and  $D_{n+2p}^n(\alpha)$  must be defined as follows:

$$B_{n+2p}^n(\alpha) = \int_{-\pi}^{\pi} \int_{Z_L}^{Z_u} G(Z, \theta) \cos n\theta \, d\theta \, H_{2p+n}(\alpha Z) \, dZ \quad (9b)$$

$$D_{n+2p}^n(\alpha) = \int_{-\pi}^{\pi} \int_{Z_L}^{Z_u} G(Z, \theta) \sin n\theta \, d\theta \, H_{2p+n}(\alpha Z) \, dZ \quad (9c)$$

If the flow field disturbance is known to be essentially axisymmetric then the following simplification can be applied: (1) all the  $D_{n+2p}^n(\alpha)$  values are zero and (2) all the coefficients will be defined with  $n = 0$ . Similarly, as noted in Ref. 10, if the flow field is known to have "k" planes of symmetry, then (1) all  $D_{n+2p}^n(\alpha)$  terms are zero and (2) only the  $B_{n+2p}^n(\alpha)$  terms for  $n = 0, k, 2k, 3k$ , etc., must be evaluated. If no planes of symmetry exist, then all the  $B_{n+2p}^n(\alpha)$  and  $D_{n+2p}^n(\alpha)$  coefficients must be evaluated. The parameter  $\alpha$  in these evaluations is simply a scaling term used to accelerate the convergence of the polynomial terms.

Although this program for evaluating the interferograms of non-symmetrical flow fields (such as the one shown in Fig. 4) has been written and checked against one known analytical solution, a displaced Gaussian distribution, further checks are needed. The sensitivity of the scaling parameter,  $\alpha$ , and the effect of the number of  $B_{n+2p}^n(\alpha)$  and  $D_{n+2p}^n(\alpha)$  coefficients on the resulting density distribution must be clearly understood. Also, the fineness of the angular mesh  $\theta$  and the radial ordinate  $Z$  of the fringe pattern required to numerically evaluate

the  $B_{n+2p}^n(\alpha)$  and  $D_{n+2p}^n(\alpha)$  coefficients should be examined. In terms of the displaced Gaussian distribution, the angular increment of at least 30 deg was needed with the fringe pattern from  $-Z$  to  $+Z$  divided into 40 equal increments. A few more analytically defined fringe patterns should be formulated to test the limitations and usefulness of this inversion technique for converting interferometric results into density distributions of nonsymmetrical flow fields.

### 4.3 DATA RECORDING TECHNIQUE

In order to process the information contained in an interferogram and obtain static density distributions in a flow field, the finite fringe pattern of the flow field must be converted into an accurate digital format; that is, the coordinates of the fringe pattern and the assigned fringe number must be listed on computer cards or a magnetic tape. Past experience has shown that manually reading and recording this amount of data will, in most cases, result in errors which will compromise the final result. At the present time, a film reader with an x-y readout which automatically punches the coordinates on computer cards is utilized. Unfortunately, the x-y position of the fringe must be selected manually and the fringe number assigned. Obviously, some judgment must be involved in selecting the center of a fringe line in an interferogram. The probable error in consistently locating the fringe center was no more than  $\pm 5$  to 10 percent of the nominal fringe spacing. In some cases, the fringe spacing in terms of the flow field dimensions can approach spacings as close as 0.04 to 0.05 in. in terms of the actual flow field disturbance. The primary difficulty in reading an interferogram is associated with keeping track of the number assigned to a particular fringe. The flow field disturbance tends to shift and collapse the spacing between fringe lines.

An attempt was also made to utilize a digital scanning microdensitometer to record the film image on magnetic tape. Although this densitometer assigned density or optical gray levels from zero to 256, the data was reprocessed and programmed to print out only the location of each successive high- and low-density level encountered as the microdensitometer scanned the negative. A further refinement to the technique was achieved by locating only the minimum density levels which varied by more than  $1/30$  from a previously located peak density level. The result is shown in Fig. 14 and corresponds to the interferogram shown in Fig. 11.

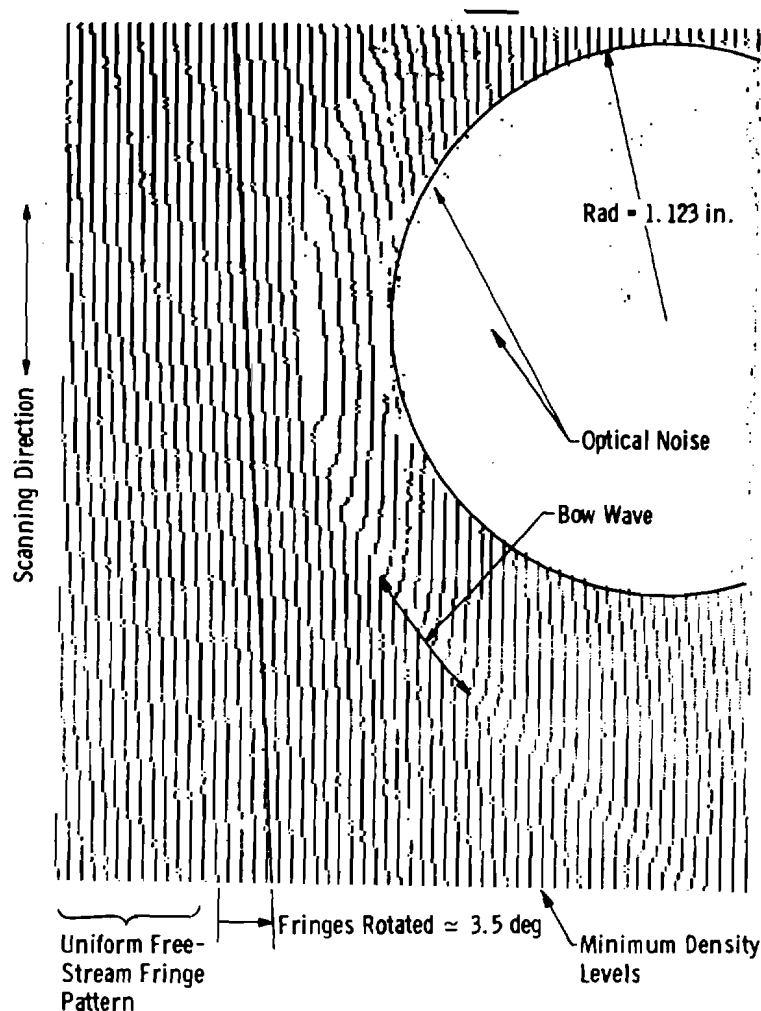


**Figure 14. Digitized fringe pattern of the flow over a sphere ( $M_\infty = 2.50$  and  $Re/ft = 9.3 \times 10^6$ ).**

Figure 14 is the image as reconstructed by a programmed output on the VKF graphic computer terminal. The body is a sting-supported, 2.247-in.-diam smooth sphere in the VKF Tunnel D operating at Mach number 2.5 with a free-stream Reynolds number of  $9.3 \times 10^6$  per foot. The scan direction of the microdensitometer is indicated on this figure and runs parallel to the undisturbed or reference fringe lines. As indicated, the angle between the scan direction and the fringe pattern is nominally 3.5 deg. In determining the maximum and minimum optical density levels, the program scans the data matrix 90 deg with respect to the microdensitometer scan direction. Changing the scan direction of the microdensitometer had little effect on the reconstructed image.

Although this technique was not pursued because of time limitations, there is no doubt that the technique would be a useful, more reliable and accurate method of rapidly digitizing interferometric results than the film-reader technique now used in the VKF. One 4- by 5-in. film negative could be scanned and recorded on tape in less than one or two minutes.

There now exists, on the commercial market, electronic photo digitizing equipment which might be adapted for use in recording the coordinates of an interferometric fringe pattern. The field of view is recorded by means of a special image dissector tube which divided the picture area into a 1000- by 1000-point matrix with a gray scale optical density range of 256 levels. These units could be programmed to follow and record on magnetic tape the coordinates of a fringe line. If the fringe pattern becomes somewhat obscure or undefined, an option to override the automatic programmed scanning sequence exists. These photo digitizing units could be programmed to track and read other forms of optically generated film data such as temperature sensitive phosphor paint data recorded on film (including the option of subtracting a reference image from the data image), the melt line of phase-change paint pictures, the trajectory locations or movement of a body photographed on high-speed movie film, or the orientation of a model or object on a film frame. Some of these photo digitizing units consist of a video camera with a special image dissector tube, a power unit, a control unit, a scan converter, and a memory digital processor.

#### 4.4 INTERFEROMETRIC LIMITATIONS

There are certain basic limitations to the practical application of interferometry in the VKF test units. Aside from those limitations attributed to the environment around a large wind tunnel such as tunnel-generated vibration, optical noise, etc., which have been somewhat circumvented by using a pulsed laser, there are limitations directly related to the static density levels in the wind tunnel stream. The magnitude of the shift in a fringe pattern is proportional to the magnitude of the change in density ( $\Delta\rho$ ) in the optical path length ( $\Delta Z$ ), that is

$$\Delta F = (K/\lambda) \Delta\rho \Delta Z$$

Assuming the minimum discernible shift in a fringe is 0.01 in. as viewed on a film reader with magnifying power of 10 and an incremental change in the optical path length of 0.10 in. (that is the ratio  $F:\Delta Z = 1:10$ ), then the sensitivity of the interferometry is qualitatively reflected by the results shown in Figs. 15 and 16. As the optical path length decreases,



as it might be when viewed in terms of the boundary layer on a body of revolution, then the local flow field density must be increased significantly to produce a measurable fringe shift. This simple analysis indicates, as expected, that the change in static density (or pressure) required to produce a measurable shift in the fringe increases significantly with the free-stream Mach number and with the free-stream total pressure. These results show that at some VKF tunnel operating conditions it becomes impractical to use interferometry in Tunnels B and C to sense variations in the local stream static density. Since the fringe shift is proportional to the optical path length, obviously an increase in model size or the use of two-dimensional models (particularly at the higher free-stream Mach numbers) improves the sensitivity of the interferometry. It is interesting to note that this requirement to sense a fringe shift is barely met at Mach number 8.0 at the minimum tunnel stagnation pressure with a normal shock in the flow field (see Fig. 15). Flow field deflections of nearly 2 deg are required at Mach numbers 8.0 and 10.0 at the maximum stagnation conditions to meet this assumed minimum fringe shift condition are shown in Fig. 16.

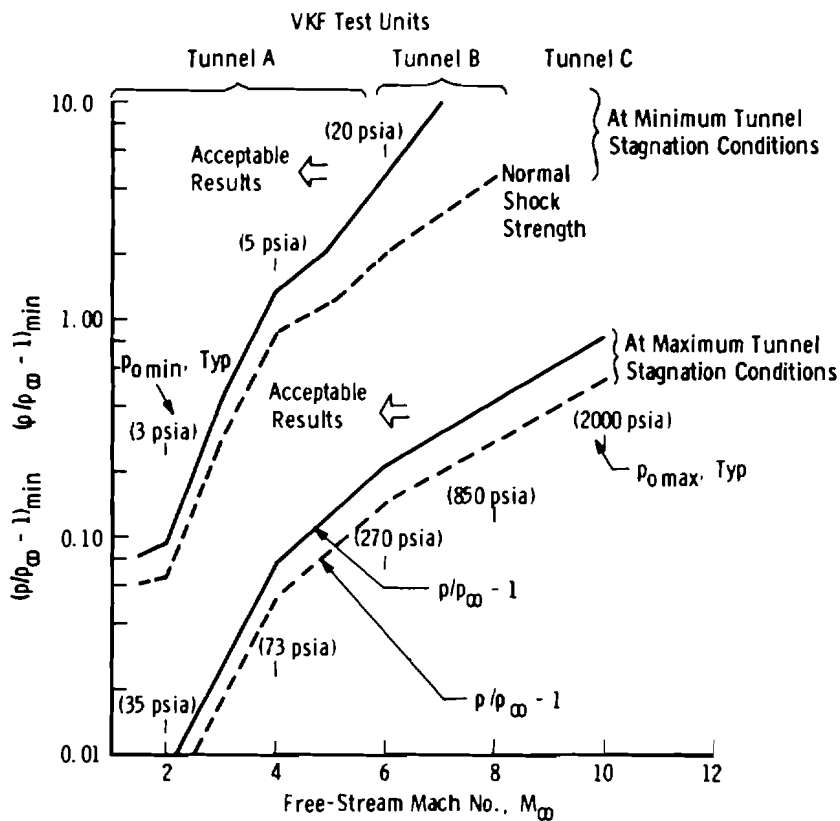
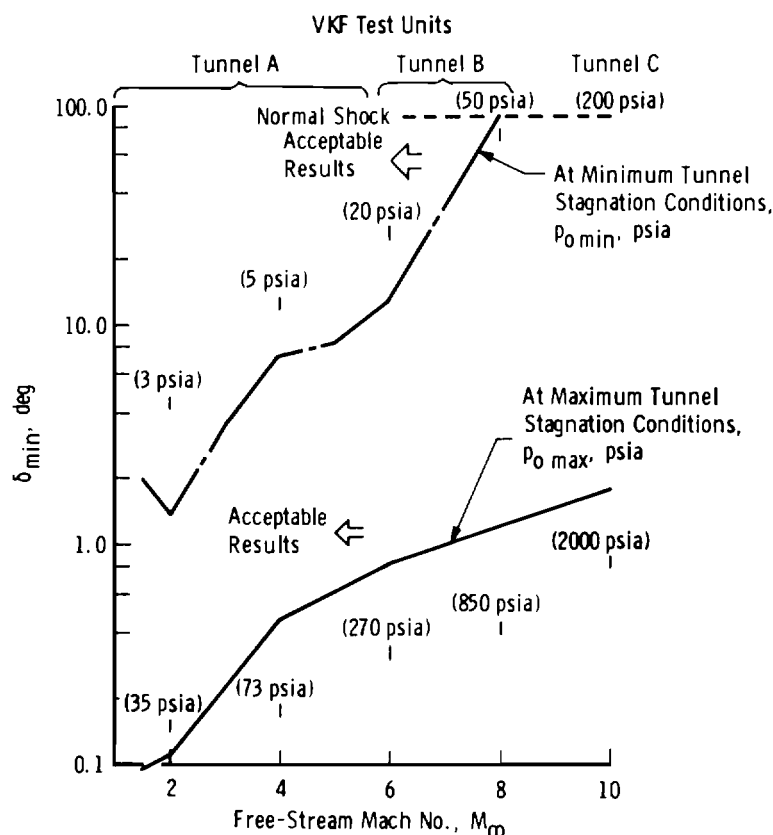
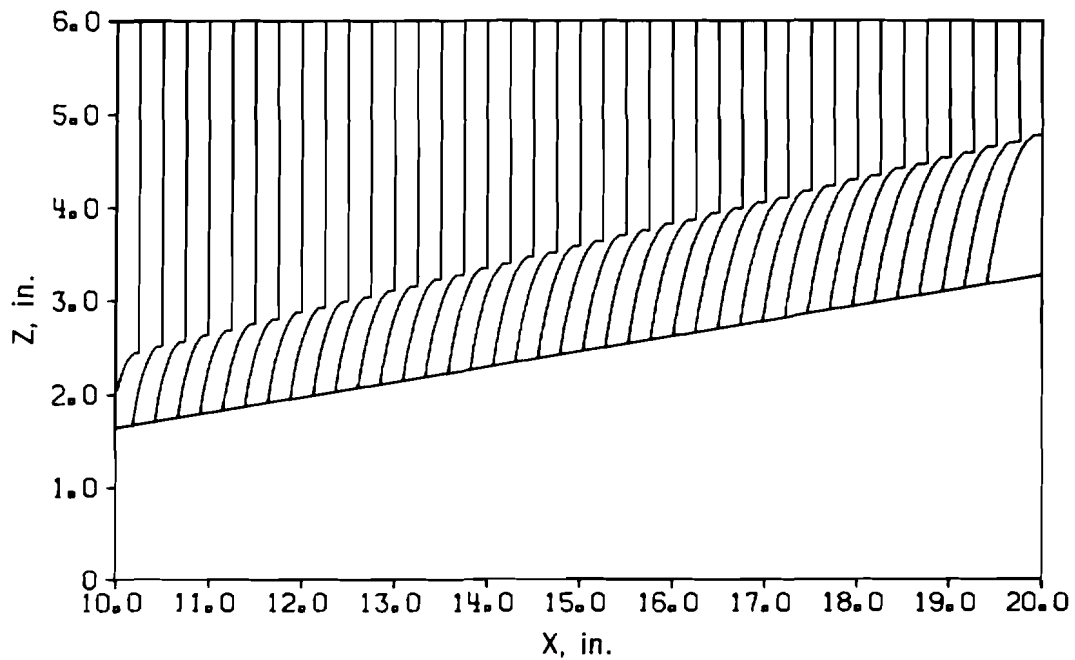


Figure 15. Minimum shock strength required assuming flow field disturbance produced an optical path length to fringe shift ratio of ten.

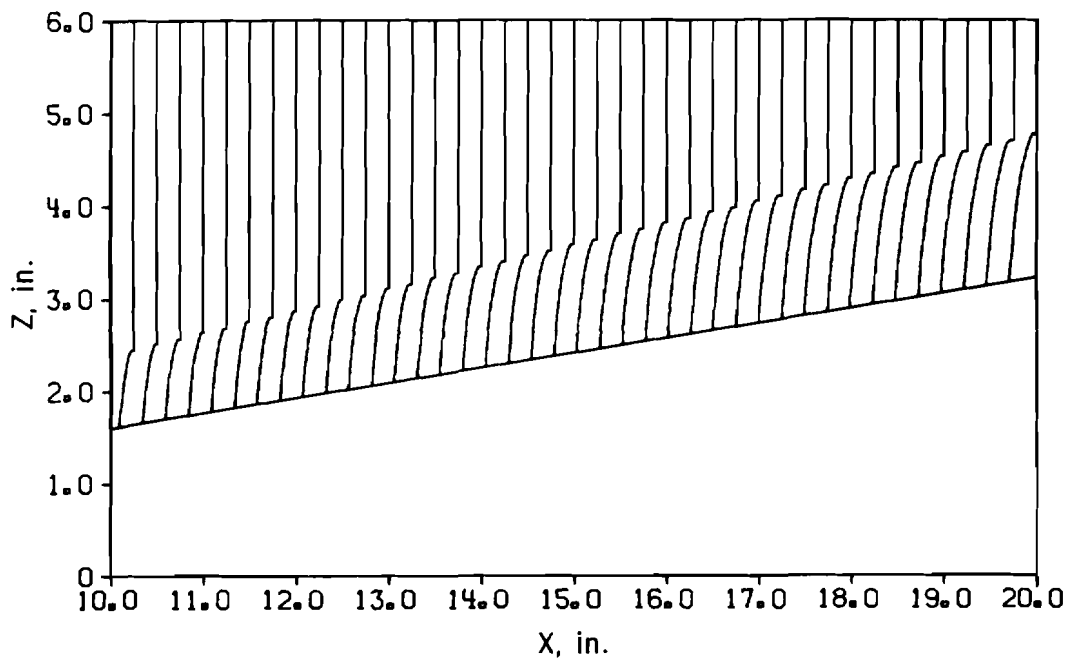


**Figure 16. Minimum flow deflection angle required assuming flow field disturbance produced an optical path length to fringe shift ratio of ten.**

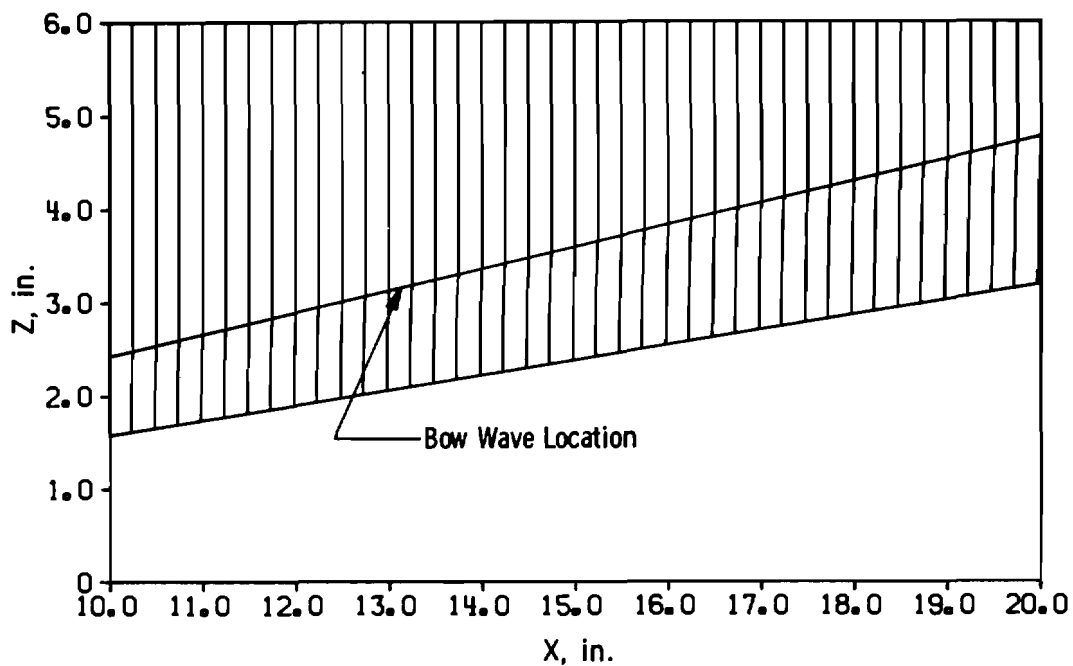
A few illustrations of the theoretical effect of tunnel operating conditions and Mach number on a finite fringe interferogram of the flow past a cone in a hypersonic stream are shown in Fig. 17. The predicted fringe patterns were based on the theoretical variation in the static density through a conical flow field and the integral expression given by Eq. (1) to define the fringe shift as a function of the assumed local static density distribution. A computer program was used to properly scale and plot the resulting fringe shift pattern on the VKF graphic computer terminal. These results in conjunction with the hypothetical limitations in the use of interferometry suggested in Figs. 15 and 16 might be used in estimating, qualitatively, the practical limitations of this optical technique. For example, a fairly reasonable fringe image of the flow over a 9-deg cone would be obtained at Mach number 6.0 in Tunnel B at the maximum tunnel condition (Fig. 17a), but at the minimum tunnel condition (Fig. 17c) the fringe shift is undiscernible. These computations were performed for a 9-deg cone which is 20 in. long, and only the theoretical fringe shift obtained over the last 10 in. of the model is shown in these results.



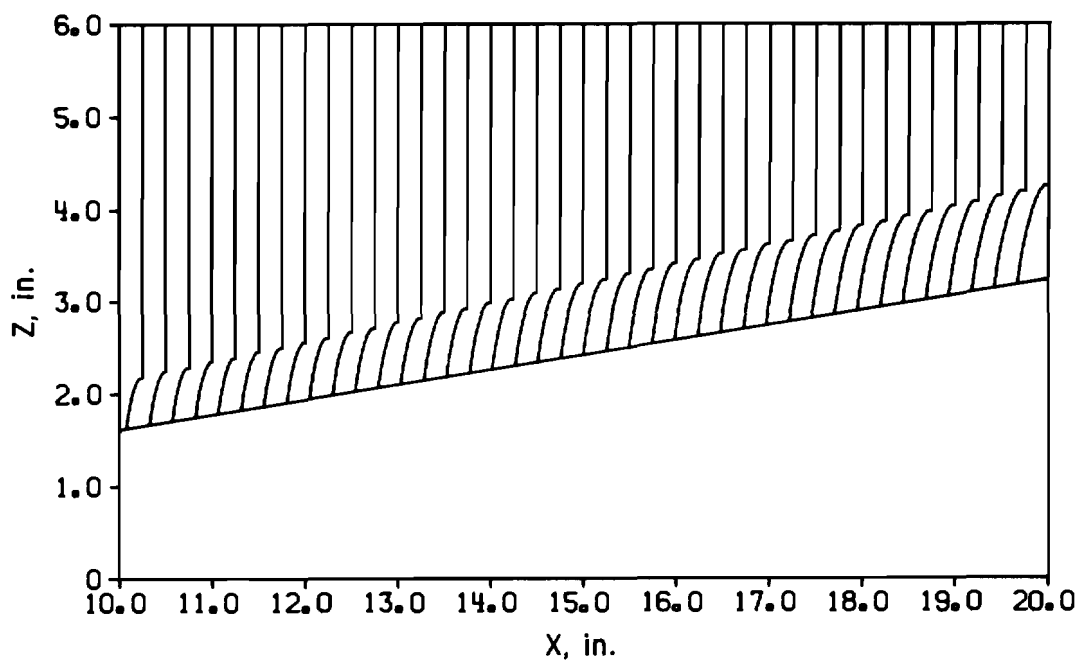
a. 9-deg cone,  $M_\infty = 6.0$ ,  $p_o = 300$  psia,  $T_o = 780^\circ\text{R}$ , and  $\text{Re}/\text{ft} = 6.3 \times 10^6$ .



b. 9-deg cone,  $M_\infty = 6.0$ ,  $p_o = 150$  psia,  $T_o = 780^\circ\text{R}$ , and  $\text{Re}/\text{ft} = 3.1 \times 10^6$ .  
 Figure 17. Analytically defined finite fringe pattern produced by a 9-deg cone in a hypersonic stream at  $\alpha = 0$  using a light source with a wave length ( $\lambda$ ) of  $0.6943 \mu$ .

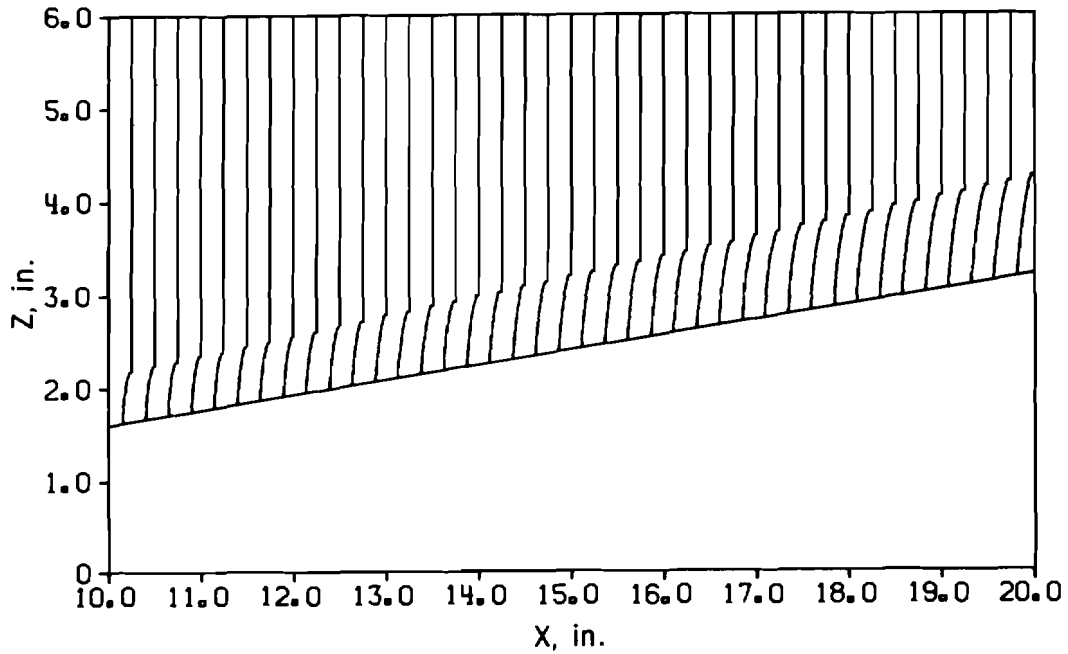


c. 9-deg cone,  $M_\infty = 6.0$ ,  $p_o = 20$  psia,  $T_o = 780^\circ\text{R}$ , and  $\text{Re}/\text{ft} = 0.4 \times 10^6$

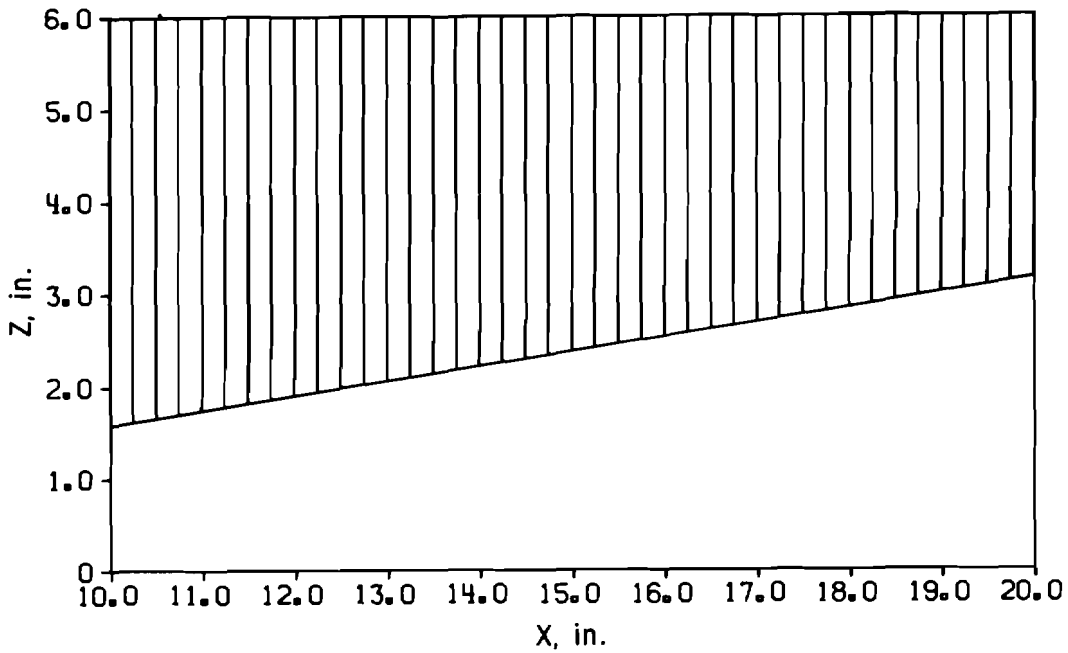


d. 9-deg cone,  $M_\infty = 8.0$ ,  $p_o = 900$  psia,  $T_o = 1320^\circ\text{R}$ , and  $\text{Re}/\text{ft} = 4.0 \times 10^6$

Figure 17. Continued.

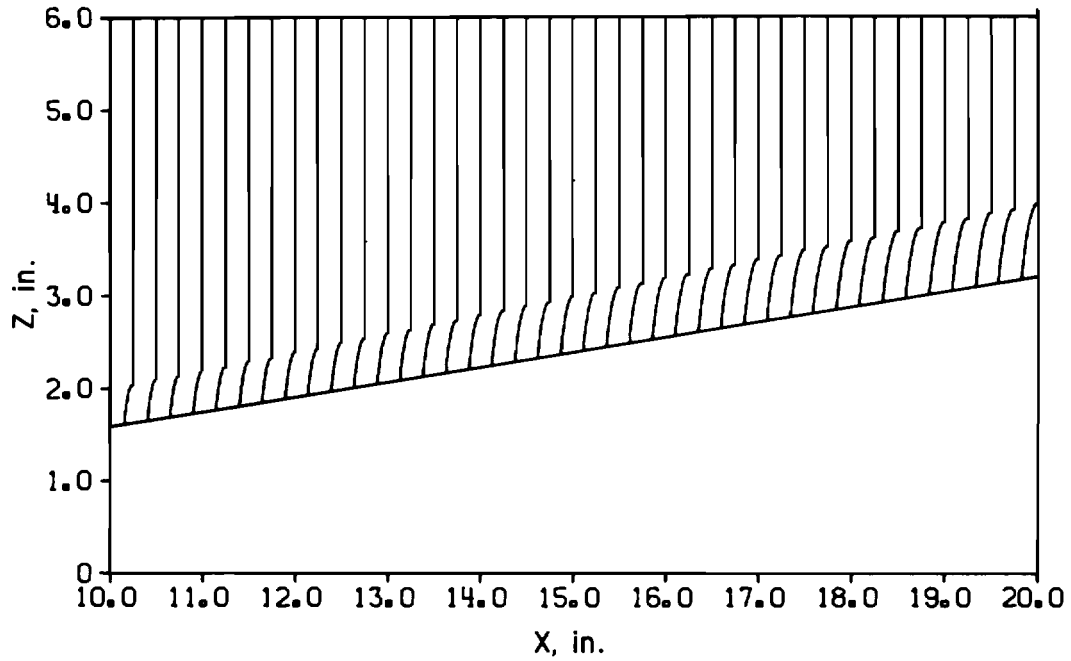


e. 9-deg cone,  $M_{\infty} = 8.0$ ,  $p_0 = 500$  psia,  $T_0 = 1320^{\circ}\text{R}$ , and  $\text{Re}/\text{ft} = 2.3 \times 10^6$

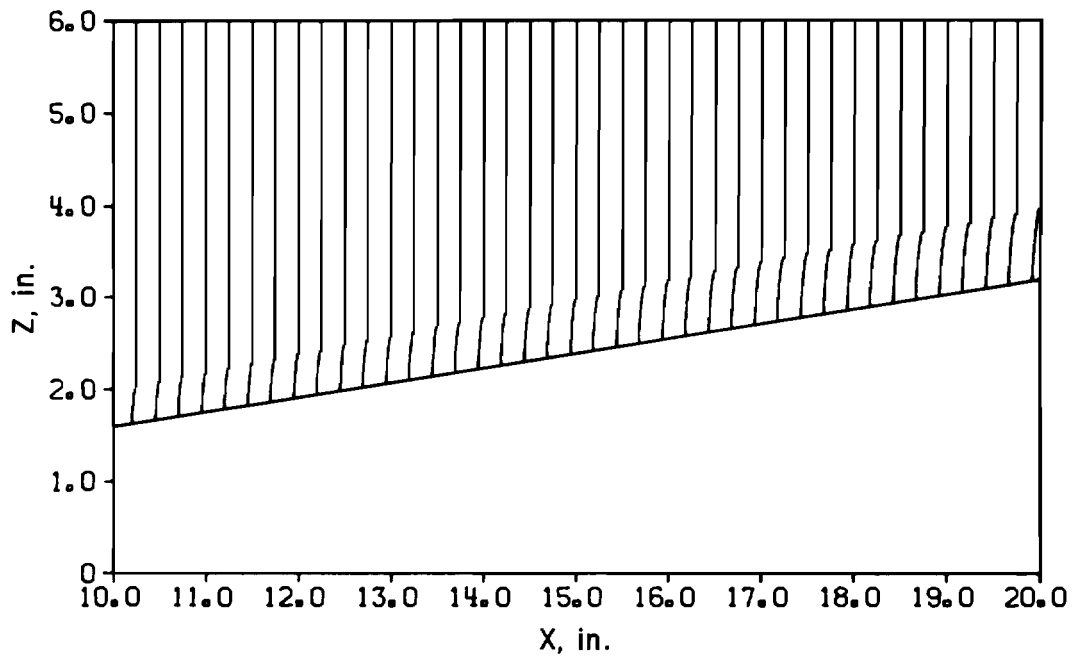


f. 9-deg cone,  $M_{\infty} = 8.0$ ,  $p_0 = 50$  psia,  $T_0 = 1320^{\circ}\text{R}$ , and  $\text{Re}/\text{ft} = 0.3 \times 10^6$

Figure 17. Continued.



g. 9-deg cone,  $M_\infty = 10.0$ ,  $p_o = 2000$  psia,  $T_o = 2000^\circ\text{R}$ , and  $\text{Re}/\text{ft} = 2.6 \times 10^6$



h. 9-deg cone,  $M_\infty = 10.0$ ,  $p_o = 1000$  psia,  $T_o = 2000^\circ\text{R}$ , and  $\text{Re}/\text{ft} = 1.3 \times 10^6$

Figure 17. Concluded.

## 5.0 CONCLUDING REMARKS

The purpose of this research effort was to (1) improve the procedure and equipment used to reconstruct holographic images, (2) to assess the feasibility of recording three-dimensional holographic results in the wind tunnel area, and (3) to provide a computer program for evaluating finite fringe holographic interferograms of nonsymmetrical flow fields.

The first objective was achieved by adding several new elements to the reconstruction system including a new 50-mw He-Ne continuous wave laser, a new double-plate holder, and a diffraction limited collimator and spatial filter for the holograms. The addition of these elements along with modifications to the Q-switched ruby laser improved the quality of the reconstructed images and significantly reduced the time required to process useful photographic results.

The second objective was only partially achieved in that several holographic techniques for recording three-dimensional optical data were examined but with only limited success. Some of these methods with further development might prove to be useful in recording flow field phenomena. One of the most promising developments was a technique involving the use of a beaded reflective material to holographically record the flow field disturbance in the shadow region of a model (e. g., the flow field disturbance in the region of the wing-fuselage junction of a model). An improvement in this technique might be achieved by using a double-plate method similar to the one now employed using direct light source illumination to produce fringe patterns, that is, using a reference image to optically interfere with the image produced by the flow field disturbance.

The third and final objective of this effort, to write a program for evaluating interferograms of nonsymmetrical flow fields, was completed. A preliminary check has shown that the program logic and numerical scheme are correct. Further checks must be made and an evaluation of the accuracy of the numerical integral inversion technique must be made before the program can be made fully operational. The range of application of this numerical scheme will depend on the number of data points required to define the final solution, the sensitivity of the scaling parameter ( $\alpha$ ) on the final result, and the minimum number of coefficients required in the polynomial expression to define the static density distribution. A variety of known or assumed nonsymmetrical

density distributions with analytically defined fringe patterns must be formulated and used as input data to this program to thoroughly check its reliability.

At the present time, the only optical holographic technique that can be used reliably in the VKF to quantitatively define the static density distribution in a flow field involves the use of a coherent, directly illuminated light source from a pulsed ruby laser. The present pulsed ruby laser is acceptable for use in producing conventional holographic interferograms, but it is inadequate for use in producing diffuse-light, three-dimensional holographic results in the wind tunnel area on a standard operational basis. The quality of these holographic applications might be improved significantly with lasers having longer and, preferably, adjustable pulse lengths.

Two general techniques now exist for reading interferograms in the VKF. A film reader with digitized card punch capability is available but unfortunately is very time consuming and can lead to recording errors. Another method involving the use of a digital scanning microdensitometer to record the film image on magnetic tape has been successfully used. A few very minor programming refinements in this method must be made before this recording procedure will be operational. A third possible scheme would involve the purchase of a programmable, electronic photodigitizing unit which is now available on the commercial market. Assuming an unusually great demand to analyze a large number of interferograms, this type of equipment would be very useful.

## 6.0 RECOMMENDATIONS

In the near future, the ability of a test facility to produce useful test results without disturbing the flow field with a probe or some other measuring device will be more common. This study has involved the development of such an experimental technique and leads to the following recommendations:

1. A new state-of-the-art laser with an adjustable pulse length from  $10^{-9}$  to  $10^{-6}$  seconds will be needed before any significant headway can be made to develop such optical methods as the diffuse-light, three-dimensional holographic technique.



2. Efforts to check out the present program used to evaluate interferograms for nonsymmetrical flow fields should be continued until its capabilities and limitations are thoroughly defined.
3. The efforts to develop three-dimensional, diffuse-light laser holography should be continued with particular emphasis placed on those methods involving the use of reflective surfaces similar to Scotchlite.
4. The technique of using the digital scanning micro-densitometer to record the fringe pattern of an interferogram should be pursued and efforts to purchase a commercially developed, programmable, photo-digitizing unit should be delayed for the time being.

## REFERENCES

1. O'Hare, J. E. "A Holographic Flow Visualization System." Symposium Proceedings, SPIE 14th Annual Technical Symposium, San Francisco, California, August 11-14, 1969.
2. O'Hare, J. E. and Trolinger, J. D. "Holographic Color Schlieren." Applied Optics, Vol. 8, No. 10, October 1969, pp. 2047-2050.
3. Trolinger, J. D. and O'Hare, J. E. "Aerodynamic Holography." AEDC-TR-70-44 (AD709764), August 1970.
4. Trolinger, J. D., Belz, R. A., and Farmer, W. M. "Conversion of Large Schlieren Systems to Holographic Visualization Systems." ISA 15th National Aerospace Instrumentation Symposium Proceedings, May 1969.
5. Trolinger, J. D. "Laser Instrumentation for Flow Field Diagnostics." AGARDograph No. 186, March 1974.

6. Ladenburg, R. W., Lewis, B., Pease, K. N., and Taylor, H. S. (Editors) Physical Measurements in Gas Dynamics and Combustion, Princeton University Press, Princeton, N. J., 1954, pp. 3-78.
7. Goodman, J. W. Introduction to Fourier Optics, McGraw-Hill Book Company, San Francisco, California, 1968.
8. Bradley, J. W. "Density Determination from Axisymmetric Interferogram." AIAA Journal, Vol. 6, No. 6, June 1968, pp. 1190-1192.
9. Jagota, R. C. "The Application of Holographic Interferometry to the Determination of the Flow Field Around a Right Circular Cone at Angle of Attack." Thesis, United States Naval Postgraduate School, Monterey, California, NPS-57C071111A (AD741067), December 1970.
10. Maldonado C. D. and Olsen, H. N. "New Method for Obtaining Emission Coefficients from Emitted Spectral Intensities, Part II - Asymmetrical Sources." Journal of the Optical Society of America, Vol. 56, No. 10, October 1966.
11. Maldonado, C. D. "Note on Orthogonal Polynomials Which Are "Invariant in Form" to Rotational Axes." Journal of Mathematical Physics, Vol. 6, No. 12, December 1965.

## NOMENCLATURE

$B_n$	Polynomial coefficients defined in Eq. (3)
$B_{n+2p}(\alpha)$	Coefficients usually associated with symmetrical properties of the flow field analysis, see Eq. (9b)
$D_{n+2p}(\alpha)$	Coefficients associated with nonsymmetrical properties of the flow field analysis, see Eq. (9c)
$F$	Fringe shift
$G$	Normalized fringe shift function, see Eq. (7)

$K$	Gladstone-Dale constant, ratio of the change in index of refraction to change in static density
$M_{\infty}$	Free-stream Mach number
$p$	Pressure, psia
$p_o$	Tunnel stilling chamber pressure, psia
$R$	Outer radius of the disturbance, in.
$Re$	Reynolds number (i.e., $Re/ft$ is the Reynolds number per foot)
$r$	Radial coordinate, in.
$T_o$	Free-stream stagnation temperature, °R
$X, Y, Z$	Coordinates of the fringe pattern, in.
$X', Y', Z'$	Coordinates of the density distribution, in.
$X_{Dp}$	Axial location of the static density distribution, in.
$\alpha$	Scaling parameter used in numerical inversion of Eq. (7)
$\Delta F, \Delta \rho, \Delta Z$	Incremental change in $F$ , $\rho$ and $Z$ , respectively
$\delta$	Flow field deflection angle, deg
$\theta$	Angular orientation of the fringe pattern relative to the real image coordinates, deg
$\lambda$	Wavelength of light source, microns ( $\mu$ )
$\rho$	Static density, $lbm/ft^3$
$\phi$	Angular orientation of the computed static density distribution in the flow field, deg

**SUBSCRIPTS**

$\ell$	Lower limit
$\mu$	Upper limit
$\infty$	Free-stream or undisturbed value